

Modes of the Kerr geometry with purely imaginary frequencies

Gregory B. Cook* and Maxim Zolotarev†

Department of Physics, Wake Forest University, Winston-Salem, North Carolina 27109

(Dated: July 26, 2016)

In this paper, we examine the behavior of modes of the Kerr geometry when the mode's frequency is purely imaginary. We demonstrate that quasinormal modes must be polynomial in nature if their frequency is purely imaginary, and present a method for computing such modes. The nature of these modes, however, is not always easy to determine. Some of the polynomial modes we compute are quasinormal modes. However, some are simultaneously quasinormal modes and total transmission modes, while others fail to satisfy the requisite boundary conditions for either. This analysis is, in part, an extension of the results known for Schwarzschild black holes, but clarifies misconceptions for the behavior of modes when the black hole has angular momentum. We also show that the algebraically special modes of Kerr with $m = 0$ have an additional branch of solutions not seen before in the literature. All of these results are in precise agreement with new numerical solutions for sequences of gravitational quasinormal modes of Kerr. However, we show that some prior numerical and analytic results concerning the existence of quasinormal modes of Kerr with purely imaginary frequencies were incorrect.

PACS numbers: 04.20.-q, 04.70.Bw, 04.20.Cv, 04.30.Nk

I. INTRODUCTION

The Kerr geometry, representing an isolated black hole with angular momentum, was introduced more than 50 years ago[1]. It is arguably the most astrophysically important solution of Einstein's equations, and has been extensively studied (see Ref.[2] for a recent review). In this paper, we are primarily interested in the quasinormal modes (QNMs) of the Kerr spacetime. They represent the natural resonant vibrations of the black hole and are linear perturbations with boundary conditions that demand no wave travel in from infinity or travel out of the black hole. QNMs of black holes in general have been extensively studied, and Refs.[3, 4] offer excellent reviews of the subject. The QNMs of Kerr are of great importance to the new field of gravitational-wave astronomy as they describe the late-time ring-down of a remnant black hole following some violent astrophysical event such as the collision of two black holes[5, 6]. They may also offer clues to the transition between classical and quantum gravity[7].

Our understanding of the nature of a particular set of gravitational modes of the Kerr geometry has remained confused for some time. Leaver's[8] numerical results based on the Regge-Wheeler equation[9] first suggested that certain QNMs of the Schwarzschild geometry might have frequencies that exist on the negative imaginary axis (NIA). These were found with frequencies, ω which were consistent with the algebraically special modes of Kerr in the Schwarzschild limit[10]. The frequencies of the algebraically special modes of Schwarzschild will be denoted $\omega = \Omega_\ell$ (see Eq. (4)). The algebraically special modes of Kerr are, in general, total transmission modes (TTMs).

There are two types of TTMs, distinguished by their behavior at the boundaries. If the QNM boundary conditions are changed at the black-hole boundary to demand no waves travel into the black hole, then we have “left”-TTMs (TTM_{LS}). If, instead, the QNM boundary conditions are changed at infinity to demand no waves travel out at infinity, then we have “right”-TTMs (TTM_{RS}). While the behavior of the algebraically special solutions at infinity was clear, their behavior at the event horizon was not explicitly considered in Ref. [10]. On the other hand, in Ref.[11] the author examined the first few algebraically special modes of the Regge-Wheeler equation and found them to be TTM_{RS} . Then, in Ref.[12], based on more refined numerical studies, the author found that the frequencies of certain QNMs of Kerr do, in the Schwarzschild limit, approach the Ω_ℓ . However, the author also suggested that the QNMs should disappear at the Ω_ℓ where they are replaced by the left and right TTMs. At this point, the literature suggested that both TTMs exist at the Ω_ℓ , and there was no conclusive evidence for QNMs at the Ω_ℓ . This confusion was set to rest by Maassen van den Brink[13] who rigorously proved that at the Ω_ℓ , Schwarzschild black hole modes are simultaneously QNMs and TTM_{LS} , but are not TTM_{RS} . More precisely, using the supersymmetric relationship between the Zerilli[14] and Regge-Wheeler[9] equations, he showed that the even-parity Ω_ℓ modes of the Zerilli equation are simultaneously QNMs and TTM_{LS} , while the odd-parity Ω_ℓ modes of the Regge-Wheeler equation are neither QNMs nor TTMs. This fully clarified our understanding of the modes of Schwarzschild with frequencies on the NIA, but how the modes of Kerr, when the angular momentum is non-zero, behave when their frequencies are on the NIA was still not understood. Onozawa and collaborators[12, 15] found the first clear numerical evidence that QNMs of Kerr can have frequencies that approach the NIA at locations that, while close to the Ω_ℓ ,

* cookgb@wfu.edu

† zalump8@wfu.edu

are not at the Ω_ℓ . Their results were refined in Ref. [16], where we found solutions with frequencies much closer to the NIA. These results are reproduced as part of our Fig. 10.

Continuing our exploration of the Kerr QNMs first reported in Ref. [16], we have found numerous new examples where the frequencies of sequences of QNMs (parameterized by the angular momentum of the black hole) get arbitrarily close to the NIA. We will examine these numerical results in Sec. III. As we were beginning our numerical investigations of Kerr QNMs, Yang *et al* [17, 18] and then Hod [19] reported finding a continuum of Kerr QNMs with frequencies on the NIA in the limit of small frequency $|\omega| \ll 1$ and for angular momenta near the extreme limit. However, we have observed no numerical evidence of this family of solutions.

Our goal in this paper is to develop a clear understanding of the behavior of the set of modes of the Kerr geometry which have frequencies that lie on the NIA. A brief description of our main results can be found in a shorter paper [20]. We have been primarily interested in the QNMs, but a clear understanding of these modes requires that we consider QNMs *and* TTMs. Using the framework of the confluent Heun equation, and in particular the theory of confluent Heun polynomial solutions outlined in Ref. [16], we will show that any modes with frequencies on the NIA must be polynomial. We will show that potential QNMs on the NIA fall into two categories, both of which consist of countably infinite sets of solutions at discrete values of the black hole's angular momentum. One category yields solutions that are QNMs. This category of solutions has never before been recognized. A second category of solutions is more complicated, itself split into two different behaviors. One subset of polynomial solutions are neither QNMs nor TTMs, but are an inseparable combination of QNM and TTM_L behaviors. The other subset of polynomial solutions are *simultaneously* QNMs and TTM_Ls. This subset can be considered a direct extension, to non-vanishing angular momenta, of the modes of Schwarzschild with frequencies Ω_ℓ . These special modes occur at discrete frequencies along the $m = 0$ sequences of the algebraically special modes of Kerr. Maassen van den Brink [13] argued that this would not happen except in the Schwarzschild case. We have shown this not to be true and, further, have found an additional branch of the $m = 0$ algebraically special modes of Kerr that, to our knowledge, has never before been recognized.

This paper is organized as follows. In Sec. II, we provide a very brief overview of the Teukolsky equations governing perturbations in the Kerr geometry. We also review the definitions of QNMs and TTMs. In Sec. III, we provide an overview of the new numerical results that strongly suggested to us that many QNMs with frequencies on the NIA might exist. In Sec. IV, we present the theory behind, and main results of the paper. The general formalism for the confluent Heun equation is reviewed in Sec. IV A. This is applied to the Teukolsky

radial equation in Sec. IV B, where we also demonstrate that QNMs on the NIA must be polynomial. We discuss the details of how we find potential polynomial QNMs in Sec. IV C. Then we discuss how we characterize these modes in Sec. IV D by using methods outlined by Maassen van den Brink [13]. Finally, we summarize and discuss our results in Sec. V. In particular, we discuss how our results reveal a new branch of the $m = 0$ algebraically special modes of Kerr in Sec. V A. In Sec. V B, we provide some insights into the incorrect results of Refs. [17–19] claiming to find a continuum of QNMs with frequencies on the NIA.

II. THE TEUKOLSKY EQUATIONS

Perturbations of the Kerr geometry obey the Teukolsky master equation which governs a complex function ${}_s\psi$ of spin-weight s [21]. Assuming the vacuum case, the master equation separates using

$${}_s\psi(t, r, \theta, \phi) = e^{-i\omega t} e^{im\phi} S(\theta) R(r). \quad (1)$$

The radial function $R(r)$ then satisfies the radial Teukolsky equation

$$\Delta^{-s} \frac{d}{dr} \left[\Delta^{s+1} \frac{dR(r)}{dr} \right] + \left[\frac{K^2 - 2is(r - M)K}{\Delta} + 4is\omega r - \lambda \right] R(r) = 0, \quad (2a)$$

where

$$\Delta \equiv r^2 - 2Mr + a^2, \quad (2b)$$

$$K \equiv (r^2 + a^2)\omega - am, \quad (2c)$$

$$\lambda \equiv {}_sA_{\ell m}(a\omega) + a^2\omega^2 - 2am\omega. \quad (2d)$$

Here, Boyer-Lindquist coordinates are used. M is the mass of the black hole and $a = J/M$ is the angular momentum parameter. Finally, ${}_sA_{\ell m}(a\omega)$ is the angular separation constant associated with the angular Teukolsky equation governing $S(\theta)$. With $x = \cos \theta$, the function $S(\theta) = {}_sS_{\ell m}(x; a\omega)$ is the spin-weighted spheroidal function satisfying

$$\begin{aligned} \partial_x \left[(1 - x^2) \partial_x [{}_sS_{\ell m}(x; c)] \right] \\ + \left[(cx)^2 - 2csx + s + {}_sA_{\ell m}(c) \right. \\ \left. - \frac{(m + sx)^2}{1 - x^2} \right] {}_sS_{\ell m}(x; c) = 0, \end{aligned} \quad (3)$$

where $c (= a\omega)$ is the oblateness parameter and m the azimuthal separation constant.

With appropriate boundary conditions, the Teukolsky equations can be solved to determine various modes of the Kerr geometry. For example, if we demand that no waves travel into the domain from infinity and that no

waves travel out from the black hole horizon, then the solutions of the Teukolsky equation will be QNMs. These are the natural resonance frequencies of a black hole. If we reverse one of these boundary conditions, our solutions will represent TTMs. If we demand that no waves travel into the black hole horizon, then the solutions are referred to as “left”-TTMs (TMM_L). Loosely speaking, such a wave travels out from the vicinity of the black hole and to infinity with no net reflection. If, instead, we demand that no waves travel out of the domain at infinity, then the solutions are referred to as “right”-TTMs (TMM_R). Loosely speaking, such a wave travels in from infinity and then into the black hole with no net reflection. If we reverse both QNM boundary conditions, a solution would represent a bound state which is not possible in the Kerr geometry.

QNM and TMM_L modes can be obtained when we choose $s \leq 0$, while TMM_R modes require $s \geq 0$ [21]. With $|s| = 2$, solutions represent gravitational perturbations. $|s| = 1$ gives electromagnetic perturbations, and $s = 0$ gives scalar perturbations. Half-integer values of s are also allowed.

The details of our method for computing QNMs are given in Ref. [16], where we also describe a high-accuracy study of the gravitational ($s = -2$) QNMs. We will repeat those details here only where they are directly relevant to our current investigations.

III. NUMERICAL RESULTS.

We next show several overview plots for the complex frequencies of gravitational ($s = -2$) QNMs of the Kerr geometry. In Ref. [16], we showed general results for the first 8 overtones, $0 \leq n \leq 7$, but for all modes with $2 \leq \ell \leq 16$. We also considered selected sequences with $n = 8$. In this paper, we will restrict ourselves to modes with $\ell = 2, 3, 4$, but will consider overtones up to $n = 31$. An individual solid line in these plots represents a sequence of mode frequencies parameterized by the dimensionless angular momentum of the black hole $\bar{a} = a/M$ in the range $0 \leq \bar{a} < 1$. In these figures, a dimensionless version of the mode frequency $\bar{\omega} \equiv M\omega$ is used.

Only two significant changes were made to the numerical methods[16] used in computing these results. First, the method for choosing the step size in \bar{a} when computing sequences of modes was modified to be more efficient and effective¹. The second change was to the method for choosing the truncation depth of the continued fraction used in locating the QNM frequencies².

¹ A maximum step size of $\Delta\bar{a} = 0.001$ is maintained, and refinement by bisection is controlled by comparing the change in the mode frequency, $\Delta\bar{\omega}$, between steps to the local radius of curvature of the sequence

² We now estimate the error as a function of the truncation depth and choose the depth to maintain a desired accuracy. A maximum

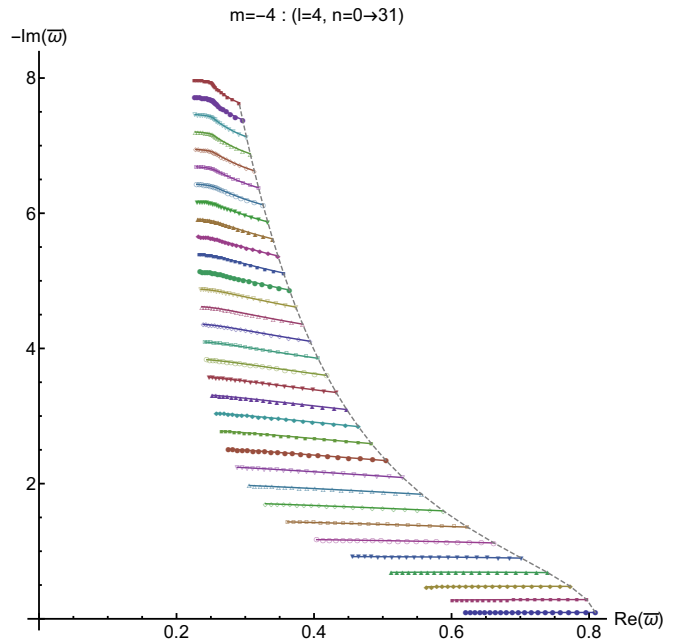


FIG. 1. Kerr QNM mode sequences for $m = -4$. The complex frequency $\bar{\omega}$ is plotted for the cases $\ell = 4$ and $0 \leq n \leq 31$. Note that the imaginary axis is inverted. Each sequence covers the range $0 \leq \bar{a} < 1$, with markers on each sequence denoting a change in \bar{a} of 0.05. The $\bar{a} = 0$ element of overtone n increases monotonically as we move up the dashed line.

Figures 1 and 2 display sequences for $\{\ell, m, n\} = \{4, -4, 0 \rightarrow 31\}$ and $\{4, 4, 0 \rightarrow 31\}$ respectively. The Schwarzschild limit, $\bar{a} = 0$, for each overtone of a given ℓ and m is connected by a dashed gray line. In the Schwarzschild limit, the overtone number increases with increasing $-\text{Im}(\bar{\omega})$. Finally, for sequences with $m > 0$ (and $\text{Re}(\bar{\omega}) > 0$), we find that many of the sequences approach an accumulation point at $\bar{\omega} = m/2$ as clearly seen in Fig. 2.

Figures 3 and 4 display sequences for $m = -3$ and $m = 3$ respectively. Each figure shows both $\ell = 3$ and 4, with overtones at the Schwarzschild limit for sequence at each ℓ connected by a dashed gray line. At the Schwarzschild limit, modes with larger values of ℓ generally have larger values of $\text{Re}(\bar{\omega})$.

Figures 5 and 6 display sequences for $m = -2$ and $m = 2$, while Figs. 7 and 8 display sequences for $m = -1$ and $m = 1$. In each of these figures, sequences with $\ell = 2, 3$, and 4 are displayed. For $\ell = 2$, the modes at the Schwarzschild limit (again connected by a gray dashed line), show a new feature. At $n = 8$ the mode becomes purely imaginary with $\bar{\omega} = \bar{\Omega}_2 = -2i$. For $m \leq 0$, the $n = 8$ sequences terminate at this frequency

imum absolute error in $\bar{\omega}$ of 10^{-8} is maintained along the sequence, but this error is decreased as necessary as adaptive refinement causes $\Delta\bar{\omega}$ between adjacent solutions to decrease.

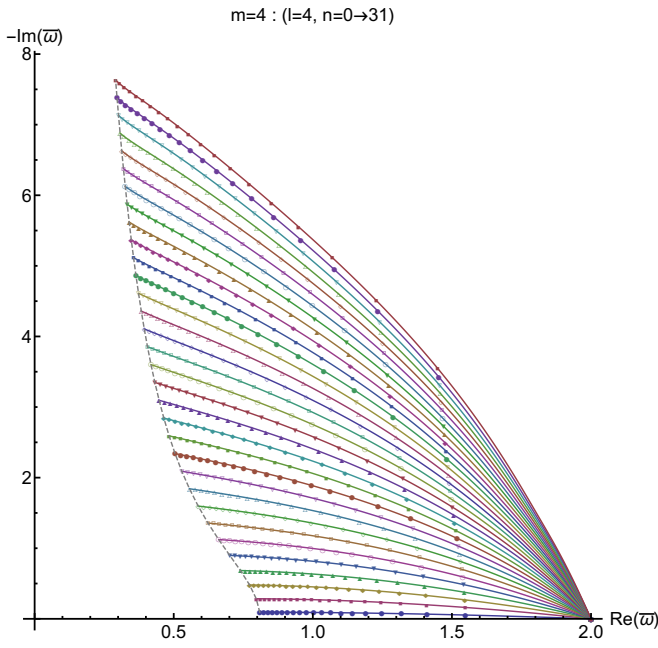


FIG. 2. Kerr QNM mode sequences for $m = 4$. See Fig. 1 for a full description. Note that as $\bar{a} \rightarrow 1$ the sequences approach an accumulation point at $\bar{\omega} = m/2$.

in the Schwarzschild limit. However, for $m > 0$ (see Figs. 6 and 8) *two* sequences in each figure approach the NIA near $\bar{\omega} = \bar{\Omega}_2$, and these sequences begin at non-vanishing values of \bar{a} . These sequences are all clearly associated with the $n = 8$ overtone. Distinct sequences that should be labeled by the same values for $\{\ell, m, n\}$ are referred to as “overtone multiplets” and are distinguished by a subscript on the overtone index ($n = 8_0$ and 8_1 in this case). We will discuss these sequences further below.

Finally, Fig. 9 displays an overview of the sequences for $m = 0$. It too shows sequences with $\ell = 2, 3$, and 4. This is a very dense figure, especially near the NIA, and we will consider it in more manageable pieces below, but we see again the same dashed gray line connecting modes at the Schwarzschild limit for $\ell = 2$ which becomes purely imaginary for $n = 8$.

A. Modes with $\ell = 2$ and $n = 8$

QNMs with $\ell = 2$ and $n = 8$ were the first computed gravitational modes with frequencies seen to approach the NIA[8, 12, 15]. All of the gravitational QNM sequences for this case are plotted in Fig. 10. Whether or not these sequences could extend to include modes with frequencies precisely on the NIA is a question which remained controversial and poorly understood until it was rigorously resolved by Maassen van den Brink[13] for modes in the Schwarzschild limit. None-the-less, subsequent works (including our own) did not fully em-

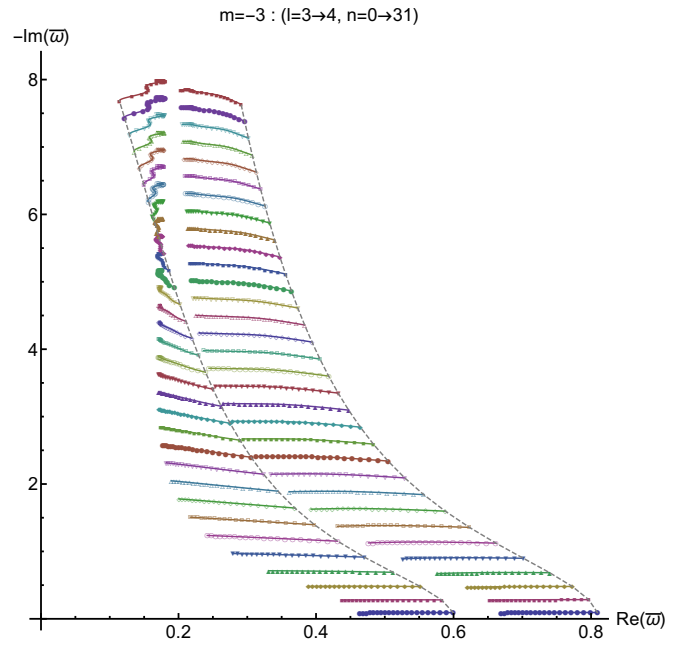


FIG. 3. Kerr QNM mode sequences for $m = -3$. See Fig. 1 for a full description. In this case, we plot the $\ell = 3$ and $\ell = 4$ sequences. Sequences with lower ℓ are generally to the left of sequences with higher ℓ .

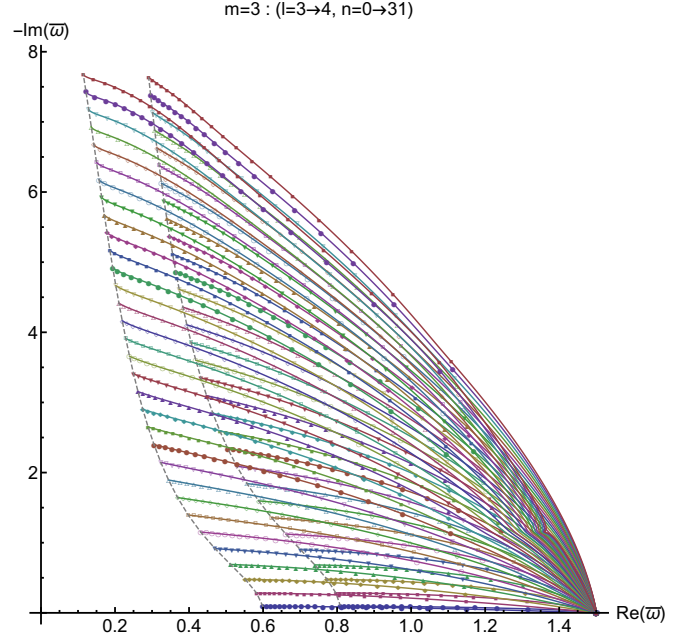


FIG. 4. Kerr QNM mode sequences for $m = 3$. See Fig. 1 for a full description. In this case, we plot the $\ell = 3$ and $\ell = 4$ sequences. Sequences with lower ℓ are generally to the left of sequences with higher ℓ . Note that as $\bar{a} \rightarrow 1$ the sequences approach an accumulation point at $\bar{\omega} = m/2$.

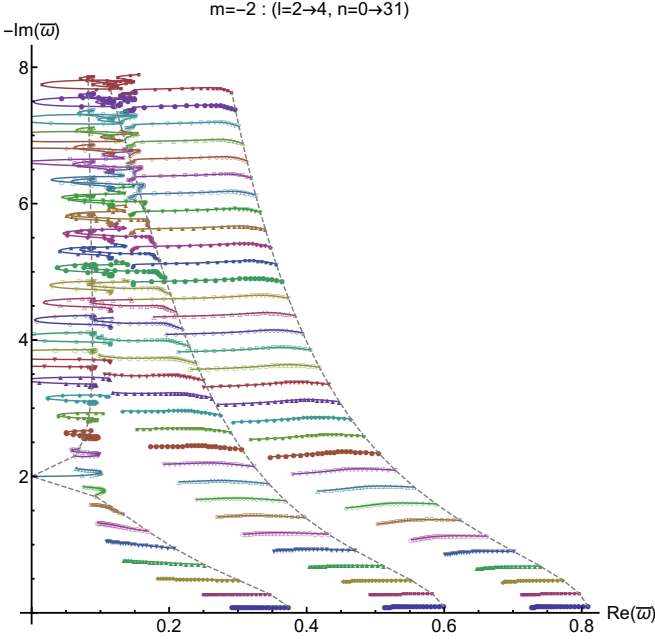


FIG. 5. Kerr QNM mode sequences for $m = -2$. See Fig. 1 for a full description. In this case, we plot the $\ell = 2$, $\ell = 3$ and $\ell = 4$ sequences. Note that several of the $\ell = 2$ sequences terminate at and re-emerge from the NIA near $\bar{\omega} \sim 4$, and several of the $\ell = 3$ sequences do the same near $\bar{\omega} \sim 7$. This behavior will be examined in more detail in Figs. 11 and 12.

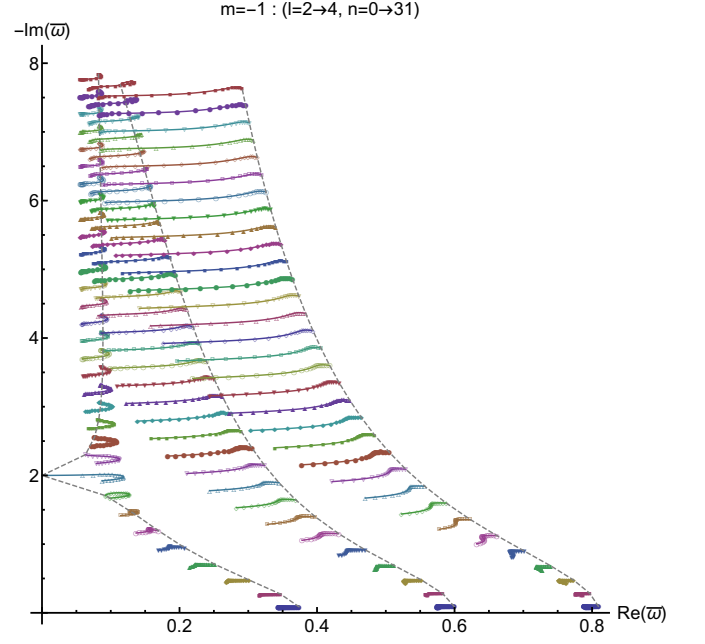


FIG. 7. Kerr QNM mode sequences for $m = -1$. See Fig. 1 for a full description. In this case, we plot the $\ell = 2$, $\ell = 3$ and $\ell = 4$ sequences.

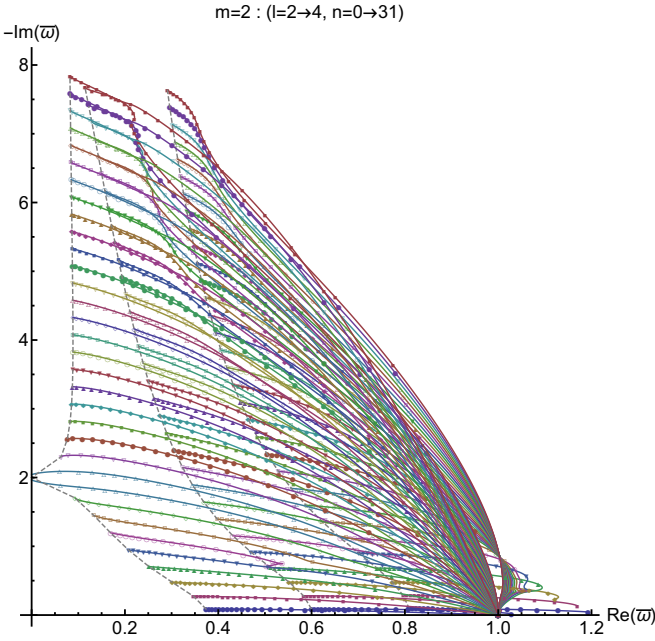


FIG. 6. Kerr QNM mode sequences for $m = 2$. See Fig. 1 for a full description. In this case, we plot the $\ell = 2$, $\ell = 3$ and $\ell = 4$ sequences. Note that as $\bar{a} \rightarrow 1$ many of the sequences approach an accumulation point at $\bar{\omega} = m/2$.

brace his findings[15, 16, 22]. However, upon gaining a fuller understanding of his approach, we now agree with Maassen van den Brink's findings. Regarding the existence of QNMs with frequencies precisely on the NIA, he finds that the algebraically special modes with frequencies $\bar{\omega} = \bar{\Omega}_\ell$, where

$$M\Omega_\ell = \bar{\Omega}_\ell \equiv -\frac{i}{12}(\ell-1)\ell(\ell+1)(\ell+2), \quad (4)$$

are QNMs. More precisely, the $s = -2$ modes are simultaneously QNMs and TTC_L s, while there is no mode in the Schwarzschild limit for $s = 2$. See Ref.[13] and [3] for further details and comments.

Furthermore, Maassen van den Brink[13] finds that a set of sequences of modes approach $\bar{\Omega}_\ell$ as $\bar{a} \rightarrow 0$. For modes with $\text{Re}(\bar{\omega}) \geq 0$, this set of sequences includes the modes with $m \leq 0$. In Fig. 10, where $\ell = 2$, we see that the $\{2, -2, 8\}$, $\{2, -1, 8\}$, and $\{2, 0, 8_0\}$ sequences appear to agree with this predicted behavior. In fact we have shown[16] that they agree quantitatively, to high accuracy, with Maassen van den Brink's predictions. For $m > 0$, he suggested several possible behaviors, none of which precisely agree with what is seen numerically[13, 15, 16, 23]. As seen in Fig. 10, the $m = 1$ and 2 sequences exist as overtone multiplets. The $\{2, 1, 8_0\}$ and $\{2, 2, 8_0\}$ sequences approach the NIA at a point slightly below $\bar{\Omega}_2$, while the $\{2, 1, 8_1\}$ and $\{2, 2, 8_1\}$ sequences approach the NIA at a point slightly above $\bar{\Omega}_2$. This behavior was first seen in Ref.[15] and confirmed in Ref.[16] where the sequences were extended to the neighborhood of the NIA with \bar{a} becoming small, but remaining finite. See Table I for numerical values of $\bar{\omega}$ and \bar{a} adjacent to the NIA.

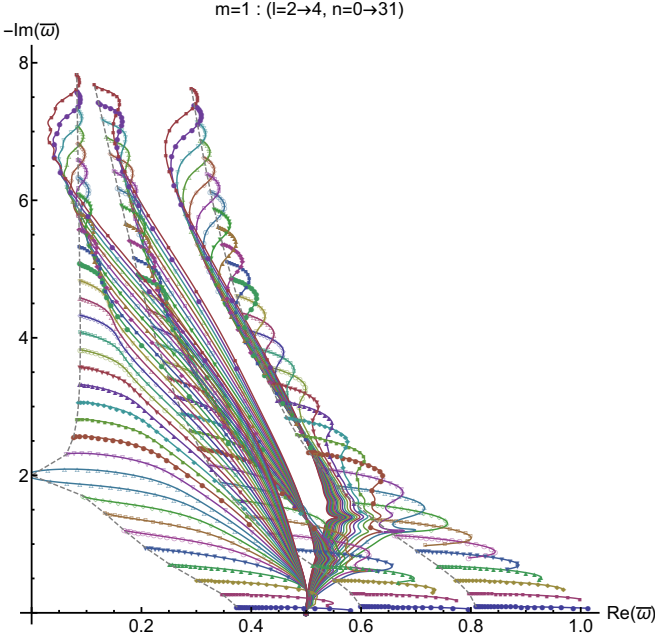


FIG. 8. Kerr QNM mode sequences for $m = 1$. See Fig. 1 for a full description. In this case, we plot the $\ell = 2$, $\ell = 3$ and $\ell = 4$ sequences. Note that as $\bar{a} \rightarrow 1$ many of the sequences approach an accumulation point at $\bar{\omega} = m/2$.

Since that work, we have found that the $m = 0$ sequence has an overtone multiplet partner. Labeled as $\{2, 0, 8_1\}$ in Fig. 10, we see that it has a spiraling shape similar to that of its partner $\{2, 0, 8_0\}$. However, similar to the $\{2, 1, 8_{0,1}\}$ and $\{2, 2, 8_{0,1}\}$ multiplets, this sequence approaches the NIA at a point displaced from $\bar{\Omega}_2$ and starts at a non-zero value of \bar{a} . See Table II for numerical values of $\bar{\omega}$ and \bar{a} adjacent to the NIA.

B. Other modes approaching the NIA

As we computed solutions at larger values of n , we encountered many other instances where sequences either approached or emerged from the NIA. In Fig. 5, we see several examples where $m = -2$ modes exist in the neighborhood of the NIA. For the case of $\ell = 2$ and $m = -2$, this behavior is seen more clearly in Fig. 11. Most of these sequences begin at the Schwarzschild limit, $\bar{a} = 0$, and smoothly move toward the extremal limit of $\bar{a} = 1$. However, for overtones $13 \leq n \leq 16$ the sequences encounter the NIA. With one exception, the sequences skip a finite range of \bar{a} where no modes are found and then reemerge from the NIA and continue toward the extremal limit. We also consider such discontinuous sequences as overtone multiplets, labeling the first segment with n_0 and the second with n_1 . See Table I for numerical values of $\bar{\omega}$ and \bar{a} adjacent to the NIA. The exceptional case is that of $n = 15$. This sequence seems to have no second segment. However, examining the general behavior of the sequences in Fig. 11, we see that the $\{2, -2, 14_1\}$ could

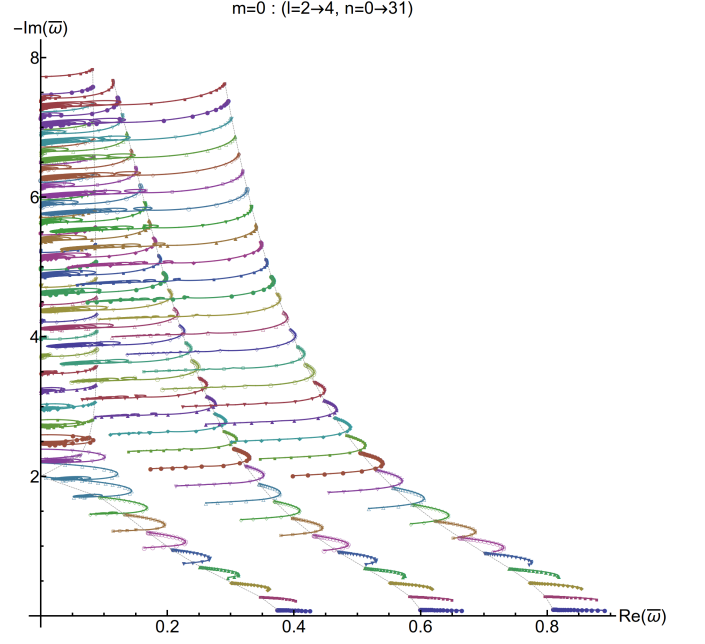


FIG. 9. Overview of Kerr QNM mode sequences for $m = 0$. See Fig. 1 for a full description. In this case, we plot the $\ell = 2$, $\ell = 3$ and $\ell = 4$ sequences. The complex behavior near the NIA will be examined in more detail in Figs. 13–18

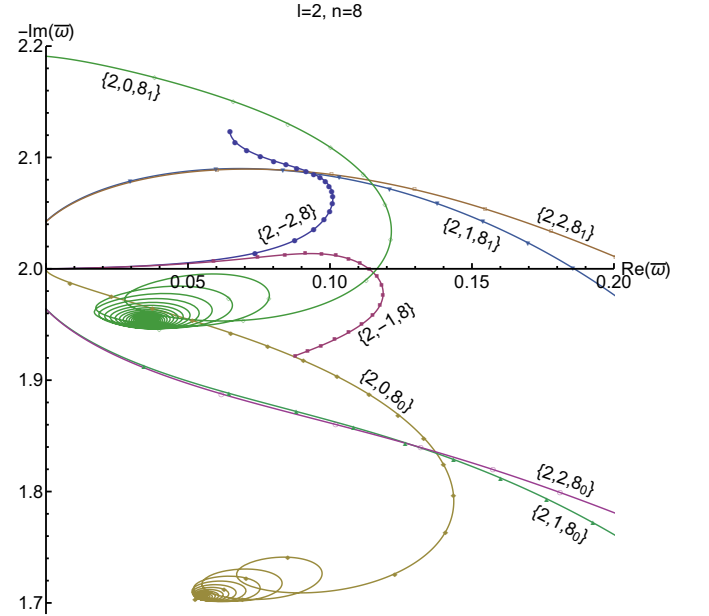


FIG. 10. Detail view near the NIA of Kerr QNM mode sequences for $\ell = 2$ and $n = 8$. See Fig. 1 for additional description. Each sequence is labeled by its values for $\{\ell, m, n\}$. Note that the $m = 0, 1$, and 2 sequences are overtone multiplets as described in the text. We will show in Sec. IV, that the 4 sequences with $m = 1$ and 2 must terminate without a mode on the NIA. The $\{2, 0, 8_1\}$ emerges from the NIA at is simultaneously a QNM and a TTM_L with a non-vanishing value of \bar{a} . The remaining 3 sequences branch out from $\bar{\omega} = -2i$ which is also simultaneously a QNM and a TTM_L with $\bar{a} = 0$.

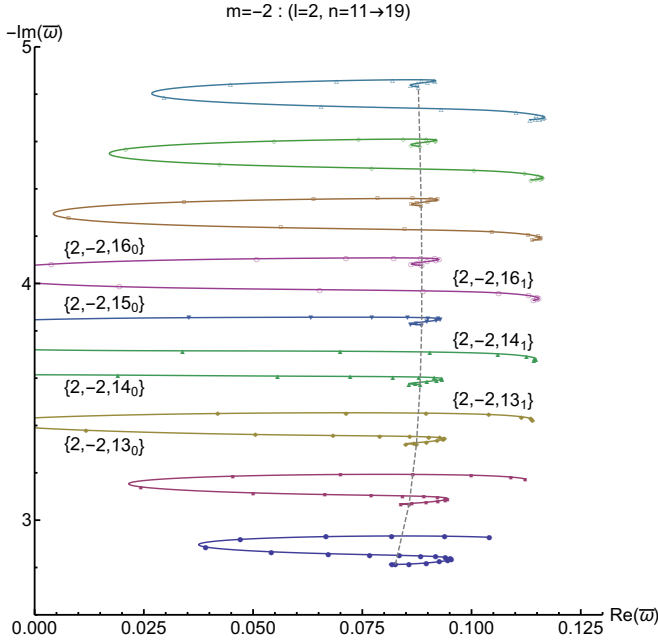


FIG. 11. Detail view near the NIA of Kerr QNM mode sequences for $\ell = 2$, $m = -2$ and $11 \leq n \leq 19$. See Fig. 1 for additional description. Each sequence is labeled by $\{\ell, m, n\}$ is part of an overtone multiplet. Sequences with a n_0 overtone terminate at the NIA, while those with a n_1 overtone re-emerge from the NIA. We will show in Sec. IV, that none of these sequences have a mode precisely on the NIA.

just as easily have been labeled as $\{2, -2, 15_1\}$, leaving $n = 14$ with no second segment. In Fig. 12 and Table I, we see similar behavior in the $\ell = 3$, $m = -2$ modes for overtones $26 \leq n \leq 29$.

As seen in Fig. 9, the vast majority of sequences that approach the NIA have $m = 0$. Figure 13 shows an expanded view containing only $8 \leq n \leq 15$. For $\ell = 2$, the first two spiraling sequences near the bottom of the plot are $\{2, 0, 8_0\}$ and $\{2, 0, 8_1\}$ discussed already in Sec. III A. For $n = 9$, we see a new behavior in the $\ell = 2$, $m = 0$ sequences. Starting at the Schwarzschild limit, the $n = 9$ sequence moves toward and terminates at the NIA at $\bar{\omega} = -2.25i$ and a finite value of \bar{a} . Following a short interval in \bar{a} with no modes, the sequence re-emerges near $\bar{\omega} = -2.39i$ and loops back towards the NIA as \bar{a} increases. However, instead of terminating again at the NIA, the sequence appears to touch the NIA at a point of tangency, continuing to loop around again. The upper right plot in Fig. 16 shows the behavior of this mode in isolation. This sequence continues through a total of 7 points of tangency before subsequent loops pull away from the NIA. Table II lists values for $\bar{\omega}$ and \bar{a} at which the sequence terminates or emerges from the NIA, while Table III lists these values for the 7 points where the sequence becomes tangent to the NIA. The data points listed in this table are the particular numerical solutions in the sequence that are closest to the NIA for each loop. Numerical solutions using Leaver's method[8, 16] cannot

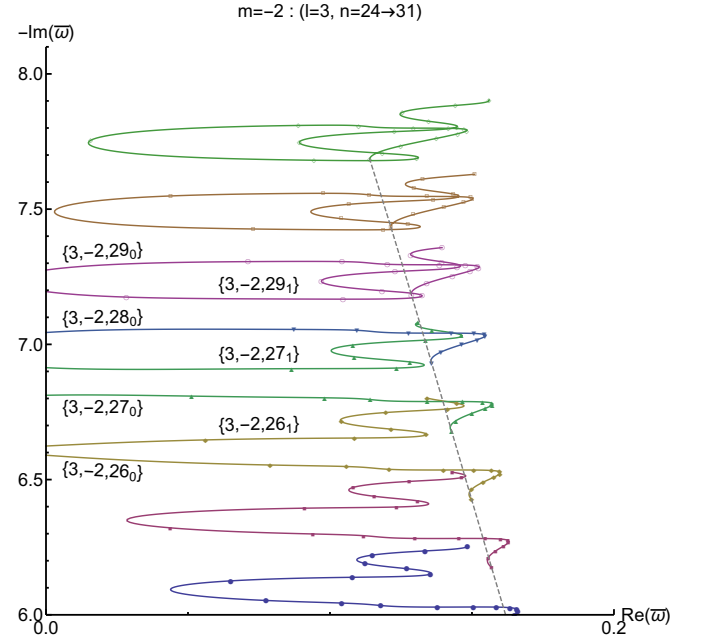


FIG. 12. Detail view near the NIA of Kerr QNM mode sequences for $\ell = 3$, $m = -2$ and $24 \leq n \leq 31$. See Fig. 1 for additional description. Each sequence is labeled by $\{\ell, m, n\}$ is part of an overtone multiplet. Sequences with a n_0 overtone terminate at the NIA, while those with a n_1 overtone re-emerge from the NIA. We will show in Sec. IV, that none of these sequences have a mode precisely on the NIA.

Mode	$\bar{\omega}$	\bar{a}
$\{2, 1, 8_0\}$	$5.38939 \times 10^{-10} - 1.96407i$	0.00688189
$\{2, 1, 8_1\}$	$2.56576 \times 10^{-10} - 2.04259i$	0.0108327
$\{2, 2, 8_0\}$	$8.05758 \times 10^{-10} - 1.96384i$	0.00348258
$\{2, 2, 8_1\}$	$3.27463 \times 10^{-8} - 2.04223i$	0.00532788
$\{2, -2, 13_0\}$	$1.00256 \times 10^{-9} - 3.38997i$	0.657472
$\{2, -2, 13_1\}$	$8.33053 \times 10^{-10} - 3.43236i$	0.669473
$\{2, -2, 14_0\}$	$6.34428 \times 10^{-10} - 3.61439i$	0.611751
$\{2, -2, 14_1\}$	$1.11866 \times 10^{-9} - 3.72003i$	0.629591
$\{2, -2, 15_0\}$	$3.82197 \times 10^{-10} - 3.84682i$	0.577994
$\{2, -2, 16_0\}$	$9.20034 \times 10^{-10} - 4.07750i$	0.552996
$\{2, -2, 16_1\}$	$8.31778 \times 10^{-11} - 4.00154i$	0.587497
$\{3, -2, 26_0\}$	$3.93481 \times 10^{-9} - 6.59006i$	0.585204
$\{3, -2, 26_1\}$	$5.75685 \times 10^{-11} - 6.62413i$	0.586625
$\{3, -2, 27_0\}$	$3.28135 \times 10^{-9} - 6.81175i$	0.563660
$\{3, -2, 27_1\}$	$5.22956 \times 10^{-9} - 6.91389i$	0.565234
$\{3, -2, 28_0\}$	$2.75891 \times 10^{-9} - 7.04384i$	0.545236
$\{3, -2, 29_0\}$	$1.55414 \times 10^{-10} - 7.27474i$	0.529576
$\{3, -2, 29_1\}$	$4.35556 \times 10^{-10} - 7.19523i$	0.543328

TABLE I. Numerical solution for QNMs closest to NIA at beginning or end of selected mode sequences. The first 4 entries correspond to sequences in Fig. 10. The next 7 entries correspond to sequences in Fig. 11. The final 7 entries correspond to sequences in Fig. 12. We will show in Sec. IV that none of these sequences can have a mode precisely on the NIA. However, our numerical results suggest that we can get arbitrarily close.

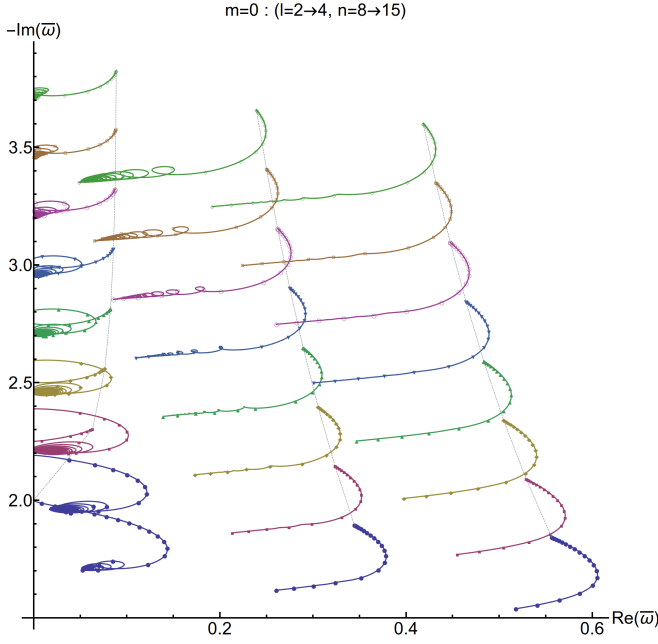


FIG. 13. Detail view near the NIA of Kerr QNM mode sequences for $m = 0$ and $8 \leq n \leq 15$. See Fig. 1 for additional description. Sequences for $\ell = 2, 3$, and 4 are shown. All of the $\ell = 2$ sequences are overtone multiplets. The $\ell = 2$ sequences also show looping behavior where many of the loops have numerous points of tangency with the NIA.

be obtained precisely on the NIA. However, quadratic interpolation confirms the points of tangency to very high precision.

For the $\ell = 2, m = 0$ sequences, a similar behavior is seen for all the sequences with $9 \leq n \leq 26$. All of these sequences are considered overtone multiplets. Figures 14 and 15 respectively show expanded views containing $16 \leq n \leq 23$ and $24 \leq n \leq 31$. The n_0 segment begins at the Schwarzschild limit and terminates at the NIA. The n_1 segments re-emerges from the NIA and performs numerous loops, many touching the NIA at points of tangency. As n increases, we see that the distance that the loops range away from the NIA decreases. In fact for $n \gtrsim 18$, the n_1 segment is nearly indistinguishable from the NIA. The lower two plot in Fig. 16 show inset plots giving expanded views of the 20_1 and 26_1 segments.

There are several interesting things to note about the n_1 segments of these sequences. First, as n increases, the number of loops that contain a point of tangency with the NIA increases rapidly. Table IV shows the number of points of tangency for each sequence for $9 \leq n \leq 17$. For $18 \leq n \leq 26$ we have not yet extended the sequence far enough to find the last loop to touch the NIA. For each sequence, we also list the values of $\bar{\omega}$ and \bar{a} for the interpolated point of tangency of the last loop that touches the NIA (or the last we have computed). Note that for $n \geq 17$, the number of loops exceeds 2000 for each sequence. Using adaptive sequencing, we have fully resolved every loop with sufficient accuracy and preci-

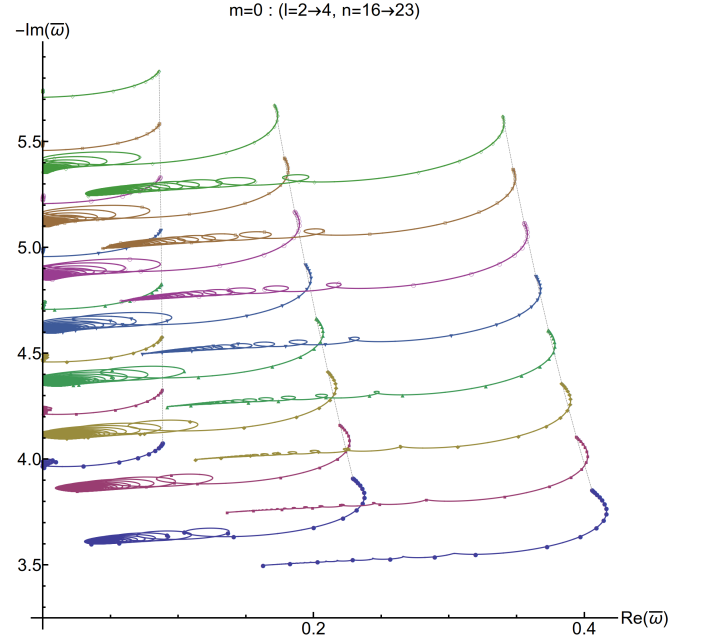


FIG. 14. Detail view near the NIA of Kerr QNM mode sequences for $m = 0$ and $16 \leq n \leq 23$. See Fig. 1 for additional description. Sequences for $\ell = 2, 3$, and 4 are shown. All of the $\ell = 2$ sequences are overtone multiplets. Many of the $\ell = 2$ and 3 sequences show looping behavior where many of the loops have numerous points of tangency with the NIA.

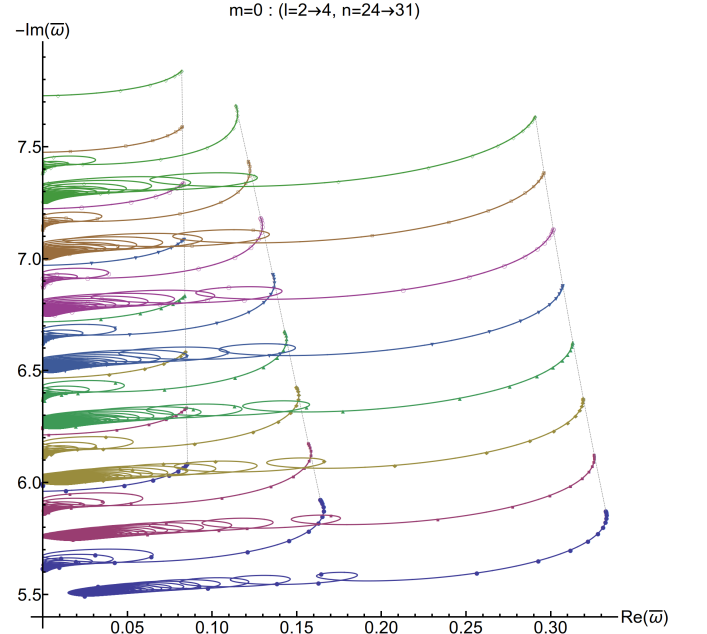


FIG. 15. Detail view near the NIA of Kerr QNM mode sequences for $m = 0$ and $24 \leq n \leq 31$. See Fig. 1 for additional description. Sequences for $\ell = 2, 3$, and 4 are shown. Only the $n \leq 26, \ell = 2$ sequences are overtone multiplets. Many of the sequences show looping behavior where many of the loops have numerous points of tangency with the NIA.

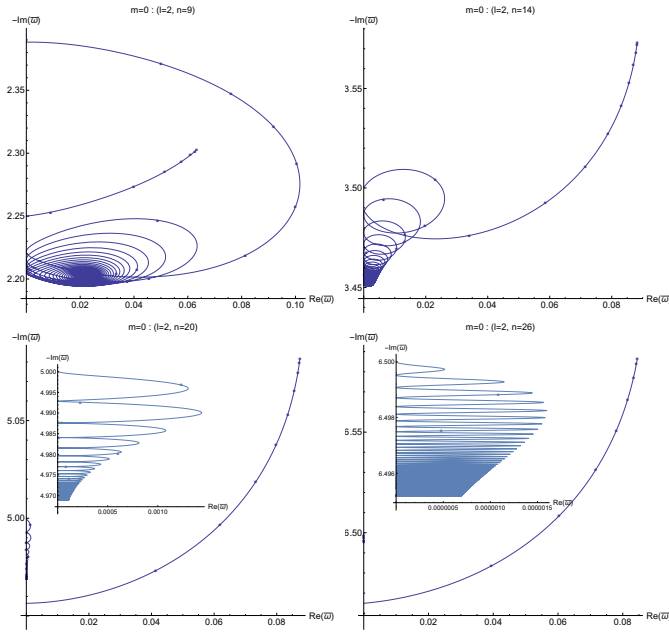


FIG. 16. Examples of $\ell = 2$, $m = 0$ modes that appear to touch the NIA. Shown are the $n = 9, 14, 20$, and 26 sequences. Each has a sequence segment that begins at the Schwarzschild limit and appears to terminate on the NIA. Each sequence re-emerges from the NIA and then repeatedly loops back with many points of tangency with the NIA. The lower two panels include insets that show an enlarged view of the second segment.

sion that we can locate each point of tangency to better than 1% of the spacing $\Delta\bar{\omega}$ between adjacent points of tangency.

For $\ell = 2$ and $n > 26$, the behavior of the sequences changes. While each sequence begins at the Schwarzschild limit and terminates at the NIA, we no longer find a second, looping segment for these sequences. We have carried out extensive searches for a second segment for $n = 27$ with no evidence for any modes with $0.4 < \bar{a} < 1$. While failing to find such modes does not prove they do not exist, we are confident in the ability of our numerical methods to find them were they to exist. Furthermore, as we will discuss in Sec. IV C, we have additional reasons to believe that sequences with $27 \leq n \leq 73$ have no second segment. This has to do with an additional curious behavior seen in the value of $\bar{\omega}$ at the NIA for one segment in each of the $\ell = 2$, $m = 0$ overtone multiplets. As can be seen in Table II and Fig. 16, for $9 \leq n \leq 13$ the n_1 segments emerge from the NIA at $\bar{\omega} = -(n/4)i$ to very high accuracy, while for the $14 \leq n \leq 26$ segments, the n_0 segment terminates at the NIA at $\bar{\omega} = -(n/4)i$. Note that the 8_0 sequence also emerges from the NIA at the corresponding value of $\bar{\omega} = -2i$.

In addition to the various $\ell = 2$, $m = 0$ sequences which show looping behavior with many points of tangency to the NIA, the $\ell = 3$ and 4 , $m = 0$ sequences also

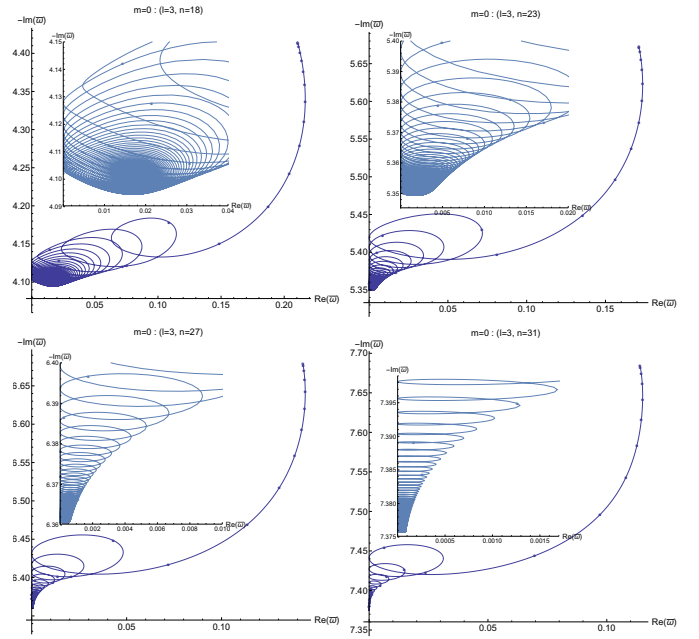


FIG. 17. Examples of $\ell = 3$, $m = 0$ modes that appear to touch the NIA. Shown are the $n = 18, 23, 27$, and 31 sequences. Each has a sequence begins at the Schwarzschild limit and then begin to exhibit loops. Many of the loops have points of tangency with the NIA. Each panel includes an inset that shows an enlarged view of the sequence near the NIA.

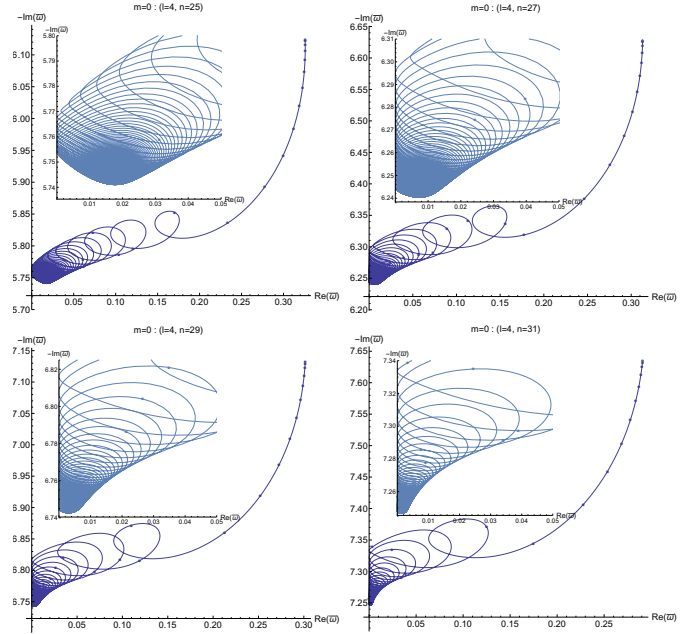


FIG. 18. Examples of $\ell = 4$, $m = 0$ modes that appear to touch the NIA. Shown are the $n = 25, 27, 29$, and 31 sequences. Each has a sequence begins at the Schwarzschild limit and then begin to exhibit loops. Many of the loops have points of tangency with the NIA. Each panel includes an inset that shows an enlarged view of the sequence near the NIA.

show a similar behavior starting with $n = 18$ for $\ell = 3$ and at $n = 25$ for $\ell = 4$. Tables III and IV also contain relevant data for the cases of $\ell = 3$ and 4. The one significant difference compared to the $\ell = 2$ case is that, so far, these sequences do not terminate at or emerge from the NIA. That is, these are all single-segment sequences. Figures 13–15 show expanded views including the $\ell = 3$ and 4 sequences, and Figs. 17 and 18 show isolated sequences with loops touching the NIA.

IV. MODES ON THE NIA

In Sec. III, we have presented significant evidence that many QNM exist with frequencies that are arbitrarily close to the NIA, but as we mention there, numerical solutions for QNMs cannot be obtained for modes precisely on the NIA when using Leaver’s method. While Maassen van den Brink[13] has answered the question of the existence of QNMs on the NIA for the special frequencies of $\bar{\omega} = \bar{\Omega}_\ell$ when $\bar{a} = 0$, we now have what seems to be a countably infinite number of modes with $\bar{a} \neq 0$ and frequencies on the NIA, and we do not know if these are QNMs.

Here, we will outline the framework needed to answer this question. We begin by looking at Leaver’s method and show why it cannot be used to compute QNMs of the Kerr geometry on the NIA. We will do this using the framework of solutions of the confluent Heun equation because the theory of confluent Heun polynomials allows us to develop a method for locating potential QNMs with frequencies on the NIA. Finally, we will examine these modes with frequencies on the NIA and describe how we determine whether or not they are QNMs.

A. Solutions of the confluent Heun equation

The confluent Heun equation is a second-order linear ordinary differential equation, obtained from the Heun equation when one regular singular point is lost by confluence with another and the point at infinity becomes irregular[24]. Written in *nonsymmetrical canonical form*, the confluent Heun equation reads

$$\frac{d^2 H(z)}{dz^2} + \left(4p + \frac{\gamma}{z} + \frac{\delta}{z-1} \right) \frac{dH(z)}{dz} + \frac{4\alpha pz - \sigma}{z(z-1)} H(z) = 0, \quad (5)$$

where the remaining two regular singular points are at $z = 0, 1$ and the irregular singular point is at $z = \infty$. It is defined by five parameters: $p, \alpha, \gamma, \delta$, and σ .

Frobenius solutions local to each of the three singular

Mode	$\bar{\omega}$	\bar{a}	N
$\{2, 0, 8_1\}$	$8.26933 \times 10^{-10} - 2.19086i$	0.315947	9
$\{2, 0, 9_0\}$	$9.85696 \times 10^{-10} - 2.25000i$	0.305661	9
$\{2, 0, 9_1\}$	$1.44669 \times 10^{-9} - 2.38829i$	0.404696	10
$\{2, 0, 10_0\}$	$2.56367 \times 10^{-10} - 2.50000i$	0.391144	10
$\{2, 0, 10_1\}$	$6.40376 \times 10^{-10} - 2.59349i$	0.451434	11
$\{2, 0, 11_0\}$	$9.02419 \times 10^{-10} - 2.75000i$	0.438874	11
$\{2, 0, 11_1\}$	$6.35257 \times 10^{-10} - 2.80677i$	0.476868	12
$\{2, 0, 12_0\}$	$6.57536 \times 10^{-10} - 3.00000i$	0.469040	12
$\{2, 0, 12_1\}$	$6.29767 \times 10^{-10} - 3.02770i$	0.489584	13
$\{2, 0, 13_0\}$	$2.82277 \times 10^{-11} - 3.25000i$	0.489617	13
$\{2, 0, 13_1\}$	$1.19986 \times 10^{-10} - 3.25539i$	0.494193	14
$\{2, 0, 14_0\}$	$2.95683 \times 10^{-10} - 3.48876i$	0.493501	15
$\{2, 0, 14_1\}$	$2.09637 \times 10^{-10} - 3.50000i$	0.504617	14
$\{2, 0, 15_0\}$	$5.24731 \times 10^{-10} - 3.72672i$	0.489333	16
$\{2, 0, 15_1\}$	$2.47748 \times 10^{-10} - 3.75000i$	0.516351	15
$\{2, 0, 16_0\}$	$4.77568 \times 10^{-10} - 3.96828i$	0.482912	17
$\{2, 0, 16_1\}$	$1.98281 \times 10^{-10} - 4.00000i$	0.526296	16
$\{2, 0, 17_0\}$	$4.02699 \times 10^{-10} - 4.21263i$	0.475069	18
$\{2, 0, 17_1\}$	$6.66620 \times 10^{-11} - 4.25000i$	0.535491	17
$\{2, 0, 18_0\}$	$6.61545 \times 10^{-10} - 4.45911i$	0.466375	19
$\{2, 0, 18_1\}$	$7.68713 \times 10^{-11} - 4.50000i$	0.544763	18
$\{2, 0, 19_0\}$	$5.31223 \times 10^{-10} - 4.70719i$	0.457216	20
$\{2, 0, 19_1\}$	$3.31607 \times 10^{-12} - 4.75000i$	0.554862	19
$\{2, 0, 20_0\}$	$9.01498 \times 10^{-10} - 4.95648i$	0.447860	21
$\{2, 0, 20_1\}$	$1.77914 \times 10^{-11} - 5.00000i$	0.566592	20
$\{2, 0, 21_0\}$	$1.98444 \times 10^{-10} - 5.20668i$	0.438486	22
$\{2, 0, 21_1\}$	$1.35783 \times 10^{-11} - 5.25000i$	0.580946	21
$\{2, 0, 22_0\}$	$1.16769 \times 10^{-9} - 5.45755i$	0.429213	23
$\{2, 0, 22_1\}$	$4.51259 \times 10^{-12} - 5.50000i$	0.599334	22
$\{2, 0, 23_0\}$	$3.28288 \times 10^{-10} - 5.70893i$	0.420123	24
$\{2, 0, 23_1\}$	$2.35358 \times 10^{-12} - 5.75000i$	0.624019	23
$\{2, 0, 24_0\}$	$4.68041 \times 10^{-12} - 5.96069i$	0.411266	25
$\{2, 0, 24_1\}$	$4.06023 \times 10^{-15} - 6.00000i$	0.659109	24
$\{2, 0, 25_0\}$	$1.80872 \times 10^{-10} - 6.21271i$	0.402672	26
$\{2, 0, 25_1\}$	$1.03997 \times 10^{-13} - 6.25000i$	0.713250	25
$\{2, 0, 26_0\}$	$1.00792 \times 10^{-10} - 6.46493i$	0.394359	27
$\{2, 0, 26_1\}$	$5.55008 \times 10^{-16} - 6.50000i$	0.808299	26
$\{2, 0, 27\}$	$3.52849 \times 10^{-10} - 6.71728i$	0.386334	28
$\{2, 0, 28\}$	$9.30984 \times 10^{-10} - 6.96973i$	0.378598	29
$\{2, 0, 29\}$	$1.06736 \times 10^{-9} - 7.22223i$	0.371147	30
$\{2, 0, 30\}$	$4.28210 \times 10^{-11} - 7.47477i$	0.363976	31
$\{2, 0, 31\}$	$5.96821 \times 10^{-10} - 7.72732i$	0.357074	32

TABLE II. Numerical solution for QNMs closest to NIA at beginning or end of selected mode sequences. The entries correspond to $\ell = 2$ sequences plotted in Figs. 13–16. We will show in Sec. IV that all of these sequences terminate at, or emerge from a mode precisely on the NIA. More than half of these are simultaneously QNMs and TTM_{LS}, however the 9₀–13₀ and 14₁–26₁ are simply QNMs. The column labeled by N contains the value for N_\pm for either Eq. (27) or (29).

points can be defined in terms of two functions[24],

$$Hc^{(a)}(p, \alpha, \gamma, \delta, \sigma; z) = \sum_{k=0}^{\infty} c_k^{(a)} z^k, \quad (6)$$

$$Hc^{(r)}(p, \alpha, \gamma, \delta, \sigma; z) = \sum_{k=0}^{\infty} c_k^{(r)} z^{-\alpha-k}. \quad (7)$$

Mode	#	$\bar{\omega}$	\bar{a}
{2, 0, 9 ₁ }	1	1.60237×10^{-9}	$-2.22167i$
	2	9.58918×10^{-10}	$-2.21540i$
	3	5.47607×10^{-10}	$-2.21151i$
	4	2.40980×10^{-10}	$-2.20889i$
	5	2.74679×10^{-10}	$-2.20705i$
	6	1.45896×10^{-10}	$-2.20569i$
	7	4.29091×10^{-11}	$-2.20466i$
{3, 0, 18}	1	3.05492×10^{-13}	$-4.12779i$
	2	2.70918×10^{-13}	$-4.12339i$
	3	9.56952×10^{-12}	$-4.11988i$
	4	1.44533×10^{-13}	$-4.11704i$
	5	1.38208×10^{-11}	$-4.11471i$
	6	1.26720×10^{-12}	$-4.11277i$
	7	1.25936×10^{-11}	$-4.11115i$
	8	3.00991×10^{-16}	$-4.10976i$
	9	4.83160×10^{-14}	$-4.10858i$
	10	1.19638×10^{-13}	$-4.10756i$
	11	3.64452×10^{-13}	$-4.10667i$
	12	3.97142×10^{-15}	$-4.10589i$
	13	5.83628×10^{-13}	$-4.10520i$
	14	2.86913×10^{-12}	$-4.10460i$
	15	2.47378×10^{-13}	$-4.10406i$
	16	5.94897×10^{-13}	$-4.10357i$
	17	1.35759×10^{-14}	$-4.10314i$
{4, 0, 25}	1	1.40943×10^{-12}	$-5.76781i$
	2	8.01725×10^{-12}	$-5.76574i$
	3	9.00602×10^{-12}	$-5.76391i$
	4	4.68881×10^{-12}	$-5.76230i$
	5	7.51494×10^{-13}	$-5.76085i$
	6	1.16406×10^{-11}	$-5.75957i$
	7	1.58023×10^{-11}	$-5.75841i$
	8	3.18629×10^{-12}	$-5.75737i$
	9	5.53437×10^{-12}	$-5.75643i$
	10	1.13290×10^{-12}	$-5.75557i$
	11	7.15779×10^{-13}	$-5.75479i$
	12	2.17820×10^{-12}	$-5.75408i$
	13	3.19872×10^{-13}	$-5.75343i$

TABLE III. Numerical solution for QNMs closest to NIA for selected sequences with loops that have points of tangency with the NIA. The first 7 entries correspond to the 7 points of tangency in the first $\ell = 2$ sequence to have such points of tangency (see upper-left panel of Fig. 16). The next 17 entries are for the corresponding first $\ell = 3$ sequences to have points of tangency to the NIA (see upper-left panel of Fig. 17). The final 13 entries are for the corresponding first $\ell = 4$ sequences to have points of tangency to the NIA (see upper-left panel of Fig. 18). We will show in Sec. IV that no QNM or TTM mode exists at any point of tangency.

Mode	N_L	$\bar{\omega}$	\bar{a}
{2, 0, 9 ₁ }	7	$-2.20466311i$	0.9366728030
{2, 0, 10 ₁ }	20	$-2.450680438i$	0.982207022698
{2, 0, 11 ₁ }	41	$-2.699696290i$	0.993545856885
{2, 0, 12 ₁ }	81	$-2.9496977199i$	0.997755524347
{2, 0, 13 ₁ }	154	$-3.2004198500i$	0.999215241283
{2, 0, 14 ₁ }	292	$-3.45173825872i$	0.999735368677
{2, 0, 15 ₁ }	555	$-3.70358925546i$	0.999913629889
{2, 0, 16 ₁ }	1058	$-3.95591591329i$	0.999972512866
{2, 0, 17 ₁ }	2036	$-4.20866196834i$	0.999991533852
{2, 0, 18 ₁ }	> 2506	$-4.4617737635i$	0.999993710751
{2, 0, 19 ₁ }	> 2826	$-4.71520182427i$	0.999994473567
{2, 0, 20 ₁ }	> 2186	$-4.9689036556i$	0.999989779470
{2, 0, 21 ₁ }	> 2363	$-5.22284221839i$	0.999990332460
{2, 0, 22 ₁ }	> 2590	$-5.47698706788i$	0.999991145753
{2, 0, 23 ₁ }	> 2860	$-5.73131247094i$	0.999992049325
{2, 0, 24 ₁ }	> 2105	$-5.98579710816i$	0.999984056118
{2, 0, 25 ₁ }	> 2487	$-6.24042211241i$	0.999987583136
{2, 0, 26 ₁ }	> 2929	$-6.49517245393i$	0.999990311150
{3, 0, 18}	17	$-4.1031415544i$	0.961319209948
{3, 0, 19}	40	$-4.3492316497i$	0.986072890543
{3, 0, 20}	75	$-4.5981480445i$	0.994372141386
{3, 0, 21}	131	$-4.84824846927i$	0.997708161178
{3, 0, 22}	225	$-5.09911272304i$	0.999072207558
{3, 0, 23}	383	$-5.35056428456i$	0.999633513815
{3, 0, 24}	652	$-5.60251180138i$	0.999857946825
{3, 0, 25}	1112	$-5.85489118443i$	0.999945856002
{3, 0, 26}	1837	$-6.10765020533i$	0.999978219330
{3, 0, 27}	> 1421	$-6.3607457778i$	0.999960719027
{3, 0, 28}	> 1694	$-6.6141303333i$	0.999970035027
{3, 0, 29}	> 1697	$-6.8677728413i$	0.999967824364
{3, 0, 30}	> 1825	$-7.1216409598i$	0.999970063305
{3, 0, 31}	> 1971	$-7.37570857244i$	0.999972448891
{4, 0, 25}	13	$-5.753433018i$	0.948986760638
{4, 0, 26}	47	$-5.995998951i$	0.983358646036
{4, 0, 27}	88	$-6.244148245i$	0.993102653036
{4, 0, 28}	151	$-6.4939321820i$	0.997042993390
{4, 0, 29}	249	$-6.7446195562i$	0.998718278044
{4, 0, 30}	404	$-6.9959315212i$	0.999450207454
{4, 0, 31}	657	$-7.2477418438i$	0.999769051122

TABLE IV. We list all of the $m = 0$ sequences with $\ell = 2-4$ and $n \leq 31$ which have loops with points of tangency to the NIA. The second column, N_L , lists the number of such points of tangency for each sequence. If the number is preceded by > then it represents the number we have computed so far, but that we have not yet found the last point of tangency for that sequence. The third column, $\bar{\omega}$, list the interpolated value for the frequency at the last point of tangency. The last column gives the corresponding interpolated value for \bar{a} .

three-term recurrence relation

$$0 = f_k^{(a)} c_{k+1}^{(a)} + g_k^{(a)} c_k^{(a)} + h_k^{(a)} c_{k-1}^{(a)} : \begin{cases} c_{-1}^{(a)} = 0, \\ c_0^{(a)} = 1, \end{cases} \quad (8a)$$

$$g_k^{(a)} = k(k - 4p + \gamma + \delta - 1) - \sigma, \quad (8b)$$

$$f_k^{(a)} = - (k + 1)(k + \gamma), \quad (8c)$$

$$h_k^{(a)} = 4p(k + \alpha - 1). \quad (8d)$$

The local solution $Hc^{(a)}(p, \alpha, \gamma, \delta, \sigma; z)$ is defined by the

At the regular singular point at $z = 0$, the characteristic

exponents (roots of the indicial equation) are $\{0, 1 - \gamma\}$ so the local solutions have the leading behavior

$$\lim_{z \rightarrow 0} H(z) \sim 1 \quad \text{or} \quad z^{1-\gamma}, \quad (9a)$$

and the two solutions local to $z = 0$ are given by

$$Hc^{(a)}(p, \alpha, \gamma, \delta, \sigma; z), \quad (9b)$$

$$z^{1-\gamma} Hc^{(a)}(p, \alpha + 1 - \gamma, 2 - \gamma, \delta, \sigma + (1 - \gamma)(4p - \delta); z). \quad (9c)$$

For the regular singular point at $z = 1$, the characteristic exponents are $\{0, 1 - \delta\}$ so the local solutions have the leading behavior

$$\lim_{z \rightarrow 1} H(z) \sim 1 \quad \text{or} \quad (z - 1)^{1-\delta}, \quad (10a)$$

and the two solutions local to $z = 1$ are given by

$$Hc^{(a)}(-p, \alpha, \delta, \gamma, \sigma - 4p\alpha; 1 - z) \quad (10b)$$

$$(z - 1)^{1-\delta} Hc^{(a)}(-p, \alpha + 1 - \delta, 2 - \delta, \gamma, \sigma - (1 - \delta)\gamma - 4p(\alpha + 1 - \delta); 1 - z). \quad (10c)$$

The solution $Hc^{(r)}(p, \alpha, \gamma, \delta, \sigma; z)$ is defined in a similar way:

$$0 = f_k^{(r)} c_{k+1}^{(r)} + g_k^{(r)} c_k^{(r)} + h_k^{(r)} c_{k-1}^{(r)} : \begin{cases} c_{-1}^{(r)} = 0, \\ c_0^{(r)} = 1, \end{cases} \quad (11a)$$

$$g_k^{(r)} = (k + \alpha)(k + 4p + \alpha - \gamma - \delta + 1) - \sigma, \quad (11b)$$

$$f_k^{(r)} = -4p(k + 1), \quad (11c)$$

$$h_k^{(r)} = -(k + \alpha - 1)(k + \alpha - \gamma). \quad (11d)$$

For the irregular singular point at $z = \infty$, the local solutions have the leading behavior

$$\lim_{z \rightarrow \infty} H(z) \sim z^{-\alpha} \quad \text{or} \quad e^{-4pz} z^{\alpha - \gamma - \delta}. \quad (12a)$$

and the two solutions local to $z = \infty$ are given by

$$Hc^{(r)}(p, \alpha, \gamma, \delta, \sigma; z) \quad (12b)$$

$$e^{-4pz} Hc^{(r)}(-p, -\alpha + \gamma + \delta, \gamma, \delta, \sigma - 4p\gamma; z). \quad (12c)$$

If a solution is simultaneously a Frobenius solution for two adjacent singular points, then the solution is called a *confluent Heun function*. In the special case that a solution is simultaneously a Frobenius solution for all three singular points, then the solution is a *confluent Heun polynomial*. A polynomial solution requires that the series solution terminates. A necessary, but not sufficient condition for this to occur is for the second parameter, α , of either Eq. (6) or (7) to be a nonpositive integer, $-\alpha$, resulting in $h_{q+1}^{(a,r)} = 0$.

If we think of the recurrence relations in Eqs. (8a) and (11a) as infinite-dimensional tridiagonal systems, then if

$h_{q+1}^{(a,r)} = 0$, we can think of the tridiagonal coefficient matrix

$$\begin{bmatrix} g_0 & f_0 & 0 & \cdots & 0 & | & 0 & 0 & 0 & \cdots \\ h_1 & g_1 & f_1 & \ddots & 0 & | & 0 & 0 & 0 & \cdots \\ 0 & h_2 & g_2 & f_2 & \ddots & | & 0 & 0 & 0 & \cdots \\ 0 & 0 & \ddots & \ddots & \ddots & | & \ddots & \ddots & \ddots & \ddots \\ 0 & 0 & \ddots & h_q & g_q & | & f_q & 0 & 0 & \cdots \\ \hline 0 & 0 & \cdots & 0 & 0 & | & g_{q+1} & f_{q+1} & 0 & \cdots \\ 0 & 0 & \cdots & 0 & 0 & | & h_{q+2} & g_{q+2} & f_{q+2} & \ddots \\ \vdots & \vdots & \ddots & \vdots & \vdots & | & \ddots & \ddots & \ddots & \ddots \end{bmatrix} \quad (13)$$

in block form. The two blocks on the diagonal are both tridiagonal. The upper-right block has only one non-zero element, f_q . The lower-left block is all zeros. The vanishing of the determinant of the upper-left block, referred to as the $\Delta_{q+1} = 0$ condition, is the necessary and sufficient condition that $c_{q+1}^{a,r} = 0$, which guarantees that the series will terminate[24].

B. The radial Teukolsky equation and Leaver's method

The radial Teukolsky equation, Eq. (2a), has regular singular points at the inner and outer horizons. These are located at the roots, r_{\pm} , of $\Delta = 0$:

$$r_{\pm} \equiv M \pm \sqrt{M^2 - a^2}. \quad (14)$$

The outer or event horizon is labeled by r_+ and the inner or Cauchy horizon by r_- . $r = \infty$ is an irregular singular point. We define the following dimensionless variables:

$$\bar{r} \equiv \frac{r}{M}, \quad (15a)$$

$$\bar{a} \equiv \frac{a}{M}, \quad (15b)$$

$$\bar{\omega} \equiv M\omega. \quad (15c)$$

In terms of the dimensionless coordinate

$$z \equiv \frac{r - r_-}{r_+ - r_-} = \frac{\bar{r} - \bar{r}_-}{\bar{r}_+ - \bar{r}_-}, \quad (16)$$

the radial Teukolsky equation, (2a), can be placed into nonsymmetrical canonical form, (5), by making the transformation

$$R(r(z)) = z^{\eta} (z - 1)^{\xi} e^{(\bar{r}_+ - \bar{r}_-) \bar{\zeta} z} H(z). \quad (17)$$

The parameters $\bar{\zeta}$, ξ , and η must be of the form

$$\bar{\zeta} = \pm i\bar{\omega} \equiv \bar{\zeta}_{\pm}, \quad (18a)$$

$$\xi = \frac{-s \pm (s + 2i\sigma_+)}{2} \equiv \xi_{\pm}, \quad (18b)$$

$$\eta = \frac{-s \pm (s - 2i\sigma_-)}{2} \equiv \eta_{\pm}, \quad (18c)$$

where

$$\sigma_{\pm} \equiv \frac{2\bar{\omega}\bar{r}_{\pm} - m\bar{a}}{\bar{r}_{+} - \bar{r}_{-}}. \quad (19)$$

See Ref.[16, 25] for a complete discussion. The parameters $\bar{\zeta}$, ξ , and η can each take on one of two values allowing for a total of eight ways to achieve nonsymmetrical canonical form, but in each case, the five parameters defining the confluent Heun equation are given by

$$p = (\bar{r}_{+} - \bar{r}_{-})\frac{\bar{\zeta}}{2} \quad (20a)$$

$$\alpha = 1 + s + \xi + \eta - 2\bar{\zeta} + s\frac{i\bar{\omega}}{\bar{\zeta}} \quad (20b)$$

$$\gamma = 1 + s + 2\eta \quad (20c)$$

$$\delta = 1 + s + 2\xi \quad (20d)$$

$$\sigma = {}_sA_{\ell m}(\bar{a}\bar{\omega}) + \bar{a}^2\bar{\omega}^2 - 8\bar{\omega}^2 + p(2\alpha + \gamma - \delta) + \left(1 + s - \frac{\gamma + \delta}{2}\right)\left(s + \frac{\gamma + \delta}{2}\right). \quad (20e)$$

When looking for QNMs, in most cases we are looking for a *confluent Heun function* which is simultaneously a local solution at $z = 1$ and at $z = \infty$. In this case, it is convenient to choose $\bar{\zeta} = \bar{\zeta}_{+}$ and $\xi = \xi_{-}$. The choice of ξ_{-} means that the solution local to $z = 1$, given by Eq. (10b), represents the desired boundary condition of no waves emerging from the black hole. The choice of $\bar{\zeta}_{+}$ means that the solution local to $z = \infty$, given by Eq. (12b), represents the desired boundary condition of no waves coming in at infinity. The choice of η is associated with $z = 0$ and is not important yet.

The desired *confluent Heun functions* are readily found using “Leaver’s method”[8, 26] which consists of removing the asymptotic behavior via $H(z) = z^{-\alpha}\bar{R}(z)$ and rescaling the radial coordinate as $z \rightarrow \frac{z-1}{z}$ so the relevant domain is $0 \leq z \leq 1$. The solution is expanded as $\bar{R}(z) = \sum_{n=0}^{\infty} a_n z^n$, resulting in a new three-term recurrence relation for the coefficients a_n :

$$0 = a_0\beta_0 + a_1\alpha_0, \quad (21a)$$

$$0 = a_{n+1}\alpha_n + a_n\beta_n + a_{n-1}\gamma_n. \quad (21b)$$

See Ref.[16] for the values of coefficients α_n , β_n , and γ_n . This new series has a radius of convergence of one and more precisely, with $r_n \equiv \frac{a_{n+1}}{a_n}$,

$$\lim_{n \rightarrow \infty} r_n = 1 + \frac{u_1}{\sqrt{n}} + \frac{u_2}{n} + \frac{u_3}{n^{\frac{3}{2}}} + \dots, \quad (22)$$

and

$$\lim_{n \rightarrow \infty} a_n \propto n^{u_2} e^{2u_1\sqrt{n}}. \quad (23)$$

See Ref.[16] for additional details. The two parameters, u_1 and u_2 take on the values

$$u_1 = \pm\sqrt{-4p} = \pm\sqrt{-2i(\bar{r}_{+} - \bar{r}_{-})\bar{\omega}}, \quad (24a)$$

$$u_2 = -\frac{1}{4}(8p - 4\alpha + 2\gamma + 2\delta + 3) \quad (24b)$$

There will be two independent series solutions to the recurrence relation, and they are distinguished by the two possible sign choices for u_1 . The QNM solution we seek will be a *minimal* solution we denote by $a_n \rightarrow f_n$, and we label the other set of coefficients by $a_n \rightarrow g_n$. A minimal solution has the property that $\lim_{n \rightarrow \infty} \frac{f_n}{g_n} = 0$. For $u_1(\bar{\omega})$, the branch cut is along the negative imaginary axis and the minimal solution corresponds to the sign choice that gives $\text{Re}(u_1(\bar{\omega})) < 0$. So long as $\text{Re}(\bar{\omega}) \neq 0$ or $\text{Im}(\bar{\omega}) > 0$, this gives $\lim_{n \rightarrow \infty} \frac{f_n}{g_n} \sim e^{-4|\text{Re}(u_1)|\sqrt{n}} = 0$ and a minimal solution will exist³. The ratio r_n can be written as a continued fraction in terms of the coefficients of the recurrence relation for the a_n .

$$r_n = \frac{-\gamma_{n+1}}{\beta_{n+1} + \alpha_{n+1}r_{n+1}} \quad n = 0, 1, 2, \dots, \quad (25a)$$

$$= \frac{-\gamma_{n+1}}{\beta_{n+1}-} \frac{\alpha_{n+1}\gamma_{n+2}}{\beta_{n+2}-} \frac{\alpha_{n+2}\gamma_{n+3}}{\beta_{n+3}-} \dots \quad (25b)$$

The key property of this recurrence relation is given by Pincherle’s theorem[27].

Theorem 1 (Pincherle) *The continued fraction r_0 converges if and only if the recurrence relation Eq. (21b) possesses a minimal solution $a_n = f_n$, with $f_0 \neq 0$. In case of convergence, moreover, one has $\frac{f_{n+1}}{f_n} = r_n$ with $n = 0, 1, 2, \dots$ provided $f_n \neq 0$.*

Since the continued fraction r_0 must converge to a specific value given by Eq. (21a), the QNM solutions are found at those frequencies $\bar{\omega}$ where r_0 does converge to this required value.

But, it is very important to recognize that for $\bar{\omega}$ on the NIA, $\text{Re}(u_1(\bar{\omega})) = 0$. Since u_1 is purely imaginary on the NIA, $\lim_{n \rightarrow \infty} \frac{f_n}{g_n}$ becomes oscillatory⁴ and a *minimal solution cannot exist unless the infinite series solution terminates*. Thus, any QNM solution on the NIA must be of the form of a *confluent Heun polynomial*. Furthermore, the continued fraction cannot be used to determine the QNM frequencies $\bar{\omega}$ on the NIA.

C. Polynomial solutions

Because confluent Heun polynomials are simultaneous Frobenius solutions of all three singular points, and the radial Teukolsky equation can be put in the form of the confluent Heun equation in eight different ways depending of the choice of the parameters $\{\bar{\zeta}, \xi, \eta\}$, the same confluent Heun polynomial can be computed in several different ways. Additional discussion of this can be found in Ref. [16] where the examples of TTM_L and TTM_R

³ Note that the discussion of the sign choice for u_1 in Ref. [16] contains an error.

⁴ Note that in the ratio $\frac{f_n}{g_n}$, the factors of n^{u_2} in Eq. (23) cancel.

polynomial solutions were examined in detail. Here, we will describe how to find QNM solutions.

Consider the boundary condition at the event horizon, $z = 1$. We must ensure that no waves propagate out from the horizon. The two local solutions at the horizon are $\lim_{z \rightarrow 1} R(z) \sim (z-1)^{-s-i\sigma_+}$, which represents waves traveling into the horizon, and $\lim_{z \rightarrow 1} R(z) \sim (z-1)^{i\sigma_+}$, which represents waves traveling out from the horizon. If we choose $\xi = \xi_-$, then the local confluent Heun solution of Eq. (10b) will achieve the first local behavior and, in general, the second behavior cannot be part of the series solution. The necessary, but not sufficient, condition for the series of this local solution to terminate is for its second parameter α to be a non-positive integer $\alpha = -q$.

Now, let us assume that we also satisfy the remaining necessary and sufficient condition, $\Delta_{q+1} = 0$. We will postpone the details of how we do that. For now, we assume we have a polynomial solution that should satisfy the boundary condition for a QNM at the event horizon. How do we know if this solution satisfies the necessary boundary condition at infinity? The key is to recall that a confluent Heun polynomial solution is *simultaneously* a polynomial solution at all three singular points. Equations (12b) and (12c) represent the two local solutions at the outer boundary, $z = \infty$. It is easy to see that the second parameter of Eq. (12b) is also α , so if we use the same set of parameters (including $\alpha = -q$) as we used to obtain the polynomial solution above, then we are guaranteed that Eq. (12b) will yield the same polynomial solutions as we obtained via Eq. (10b) above which has the desired QNM behavior at the event horizon. Now, however, using Eq. (12b) allows us to understand the behavior of the solution at the outer boundary. At the outer boundary, $z = \infty$, we must ensure that no waves enter from infinity. The two local behaviors at infinity are $\lim_{z \rightarrow \infty} R(z) \sim z^{-1-2s+2i\bar{\omega}} e^{i(\bar{r}_+ - \bar{r}_-)\bar{\omega}z}$, which represents waves traveling out at infinity, and $\lim_{z \rightarrow \infty} R(z) \sim z^{-1-2i\bar{\omega}} e^{-i(\bar{r}_+ - \bar{r}_-)\bar{\omega}z}$, which represents waves traveling in from infinity. Using Eq. (12b), the parameter choice $\bar{\zeta} = \bar{\zeta}_+$ will achieve the first local behavior and, in general, the second behavior cannot be part of the series solution.

In order to satisfy the $\Delta_{q+1} = 0$ condition, we must construct the $(q+1)$ -dimensional upper-left block of (13). With our choices of $\xi = \xi_-$ and $\bar{\zeta} = \bar{\zeta}_+$, we could use the coefficients from the recurrence relations associated with either Eq. (10b) or (12b) to construct this matrix. However, we have not yet fixed the choice for η .

At the Cauchy horizon, $z = 0$, the two local solutions are $\lim_{z \rightarrow 0} R(z) \sim z^{-s+i\sigma_-}$ and $\lim_{z \rightarrow 0} R(z) \sim z^{-i\sigma_-}$. The first behavior is associated with the local solution of Eq. (9b) if we choose $\eta = \eta_+$. Notice that the second parameter of Eq. (9b) is again α , so the same choice of parameters as above will yield the same polynomial solution satisfying the QNM boundary conditions *and* the first local behavior at $z = 0$ mentioned above. Thus, if we choose the parameter set $\{\bar{\zeta}_+, \xi_-, \eta_+\}$ and let $q = -\alpha$ be a non-negative integer, then the matrices constructed

from Eqs. (9b), (10b), or (12b) will yield the *same confluent Heun polynomial solution* if the $\Delta_{q+1} = 0$ condition is satisfied⁵.

With the parameter set $\{\bar{\zeta}_+, \xi_-, \eta_+\}$, the condition that $\alpha = -q$ can be rewritten as

$$q + s + 1 \equiv N_+ = 2i \left[\frac{2\bar{\omega} - m\bar{a}}{\bar{r}_+ - \bar{r}_-} + \bar{\omega} \right], \quad (26)$$

where $N_+ \geq s + 1$ will be either an integer or a half-odd integer depending on s . This can be rewritten as a constraint on the values of $\bar{\omega}$ that can potentially be associated with a confluent Heun polynomial solution

$$\bar{\omega} = \bar{\omega}_+ \equiv \frac{\bar{a}m - iN_+\sqrt{1 - \bar{a}^2}}{2(1 + \sqrt{1 - \bar{a}^2})}. \quad (27)$$

Now, consider the other possible choices for the parameter set $\{\bar{\zeta}, \xi, \eta\}$. Each pair of local solutions, Eqs. (9), (10), or (12), are associated respectively with the parameters η , ξ , and $\bar{\zeta}$, and each choice allows one of the pairs of solutions to yield one of the two possible local behaviors for $R(z)$. For example, if we switch our choice for η so that the parameter set is $\{\bar{\zeta}_+, \xi_-, \eta_-\}$, we can consider solutions with the same physical behaviors at all three singular points as described above if we construct our coefficient matrix using the recurrence relations associated with Eq. (9c). In this case, the necessary condition for a polynomial solution is $\alpha + 1 - \gamma = -q$, but in terms of the new parameter set this yields exactly the same constraint that $\bar{\omega} = \bar{\omega}_+$.

Alternatively, if we use the parameter set $\{\bar{\zeta}_+, \xi_-, \eta_-\}$ but construct our coefficient matrix using the recurrence relations associated with Eq. (9b) (or vi Eq. (10b) or (12b)), then we are considering a second possible set of QNM solutions where the local behavior at the Cauchy horizon has changed. In this case, the condition that $\alpha = -q$ can be rewritten as

$$q + 1 \equiv N_- = 4i\bar{\omega}, \quad (28)$$

where $N_- \geq 1$ is an integer, and we can rewrite this condition as the constraint

$$\bar{\omega} = \bar{\omega}_- \equiv -i \frac{N_-}{4}. \quad (29)$$

In total, each of the six local solutions combines with two of the eight possible choices for the parameter set $\{\bar{\zeta}, \xi, \eta\}$ to correspond to one or the other of the two possible polynomial QNM solutions distinguished by the two possible local behaviors at the Cauchy horizon. These possibilities are summarized by

$$-q = \begin{cases} \alpha & (\bar{\zeta}_+, \xi_-, \eta_{\pm}), \\ \alpha + 1 - \delta & (\bar{\zeta}_+, \xi_+, \eta_{\pm}), \\ -\alpha + \gamma + \delta & (\bar{\zeta}_+, \xi_-, \eta_{\pm}), \\ \alpha + 1 - \gamma & (\bar{\zeta}_+, \xi_-, \eta_{\mp}). \end{cases} \quad (30)$$

⁵ Satisfying the $\Delta_{q+1} = 0$ for any one of the three matrices guarantees the condition will be satisfied by the other two matrices at the same value of \bar{a}

In each case, the upper sign choice for η corresponds to a solution with the local behavior of $R(z) \sim z^{-s+i\sigma_-}$ and the necessary condition that $\bar{\omega} = \bar{\omega}_+$, while the lower sign choice corresponds to $R(z) \sim z^{-i\sigma_-}$ and the necessary condition that $\bar{\omega} = \bar{\omega}_-$. A similar analysis for the TTM_L and TTM_R cases can be found in Ref.[16].

As foreshadowed in Sec. IIIB, we note that several of the sequences approaching the NIA (see Table II) do so at a frequency $\bar{\omega} = \bar{\omega}_-$. Moreover, all of the $m = 0$ sequences we have examined which begin at, terminate at, or become tangent to the NIA satisfy either $\bar{\omega} = \bar{\omega}_+$ or $\bar{\omega} = \bar{\omega}_-$. For the $\bar{\omega}_+$ case, this requires agreement with both $\bar{\omega}$ and \bar{a} . More than half of the modes in Table II, and all of the modes in Tables III and IV satisfy the constraint $\bar{\omega} = \bar{\omega}_+$. In Table II, the value of N_\pm is listed in the last column.

The fact that so many $m = 0$ sequences are approaching the NIA at precisely the frequencies constrained by $\bar{\omega}_+$ and $\bar{\omega}_-$ gives us confidence that we are approaching polynomial solutions on the NIA. However, these conditions are only necessary, not sufficient, for the existence of polynomial solutions. To guarantee that we have found confluent Heun polynomial solutions, we must also solve the $\Delta_{q+1} = 0$ condition.

1. Solving the $\Delta_{q+1} = 0$ condition

Mode frequencies, $\bar{\omega}$, of the coupled Teukolsky equations depend only on s , m , and \bar{a} , and effectively ℓ through the choice of a particular eigenvalue ${}_sA_{\ell m}(\bar{a}\bar{\omega})$ from our solutions to the angular Teukolsky equation, Eq. (3). As we saw for general QNMs, given fixed s , ℓ , and m , the mode frequencies form sequences parameterized by \bar{a} . For the case of confluent Heun polynomials, the modes are again parameterized solely by \bar{a} . In this case, the $\Delta_{q+1} = 0$ condition effectively replaces the radial Teukolsky equation, but there is an additional constraint.

To construct the coefficient matrix for the $\Delta_{q+1} = 0$ condition, we choose one of the local Heun solutions along with the set of parameters $\{\bar{\zeta}, \xi, \eta\}$. How does the additional constraint affect our solutions? For the case of TTMs, as discussed in detail in Sec. IIIB of Ref. [16], this condition only fixes an integer value for q which fixes the size of the coefficient matrix and the order of the polynomial solutions. For the TTMs, this condition does not directly constrain the mode $\bar{\omega}$. The $\Delta_{q+1} = 0$ condition then yields an algebraic equation which turns out to be the square of the Starobinsky constant[10]. This can be solved, together with the angular Teukolsky equation, to yield the mode frequency $\bar{\omega}$ as a continuous function of \bar{a} . See Fig. 24 of Ref. [16] for plots of the various $\ell = 2$ and $\ell = 3$ TTM mode sequences.

When considering polynomial QNM solutions, we have seen that the additional constraint fixes the mode frequency as a function of \bar{a} and a new parameter N_\pm (see Eqs. (27) and (29)). The $\Delta_{q+1} = 0$ condition no longer

has the freedom to pick $\bar{\omega}$ to satisfy the condition for each value of \bar{a} . Instead, we must search for values of \bar{a} at which the $\Delta_{q+1} = 0$ condition is satisfied, subject to the constraint that $\bar{\omega} = \bar{\omega}_\pm(N_\pm, \bar{a})$. Typically, we can only expect this to yield isolated, discrete solutions instead of a continuum.

While the $\Delta_{q+1} = 0$ condition could be easily reduced to an algebraic equation for the TTM cases[16], this becomes too difficult for QNMs because the size of the matrix can get arbitrarily large depending on the value of N_\pm . Therefore, we construct the determinant of the coefficient matrix numerically and use root-finding methods to locate the zeros of the determinant. To obtain a numerical value for the determinant, we must choose values for s , m , ${}_sA_{\ell m}$, N_\pm and \bar{a} . To search for roots, we first fix s , m , and N_\pm . The determinant is then considered a function of \bar{a} with ${}_sA_{\ell m}$ chosen as follows for each value of \bar{a} .

${}_sA_{\ell m}$ is an eigenvalue of the spin-weighted spheroidal differential equation given in Eq. (3). With s and m fixed, the value of the oblateness parameter $c = \bar{a}\bar{\omega}$ is computed using the the current value of \bar{a} with $\bar{\omega}$ set via Eq. (27) or (29) as appropriate together with the fixed value of N_\pm . With all its parameters fixed, Eq. (3) is solved using the spectral method described in Ref.[16]. The solution yields an ordered set of eigenvalues that are labeled by ℓ . During any given search, we fix which element of the set of eigenvalues to use. For example, for $m = 0$ and $s = -2$, the first eigenvalue is labeled $\ell = 2$, the second by $\ell = 3$, and so on. The labeling of the eigenvalue is not absolute. Sequences of solutions, can cross depending on what criteria are used to define the sequences and so the labeling of solutions is not unique. When comparing solutions, we must be careful to compare the values of ${}_sA_{\ell m}$ and not simply (ℓ, m) index pairs.

The matrix of coefficients can be quite large. For the case of $\bar{\omega} = \bar{\omega}_+$, the matrix is $(N_+ - s) \times (N_+ - s)$. For the case of $\bar{\omega} = \bar{\omega}_-$, the matrix is $N_- \times N_-$. Since N_\pm can get large, we must be concerned about the matrix being ill-conditioned. We also find that the value of the determinant can vary over many orders of magnitude as \bar{a} varies between 0 and 1. To ensure that numerical problems are not significant, we have used two methods for computing the determinant. The first is simply to compute the determinant directly. But, we also use singular-value decomposition to decide when the matrix has a vanishing determinant.

In singular value decomposition, a matrix \mathbf{M} is decomposed as $\mathbf{M} = \mathbf{U} \cdot \mathbf{D} \cdot \mathbf{V}^\dagger$ where \mathbf{U} and \mathbf{V} are unitary matrices and \mathbf{D} is a diagonal matrix whose elements are real and non-negative. A much better behaved proxy for the determinant is to look for roots of

$$\det(\mathbf{U} \cdot \mathbf{V}^*) \min(\text{diag}(\mathbf{D})). \quad (31)$$

Using only the minimum diagonal element from \mathbf{D} keeps the function from varying so dramatically in magnitude. It is important to keep the determinant of $\mathbf{U} \cdot \mathbf{V}^*$. Even though it has unit magnitude, this term contains all of

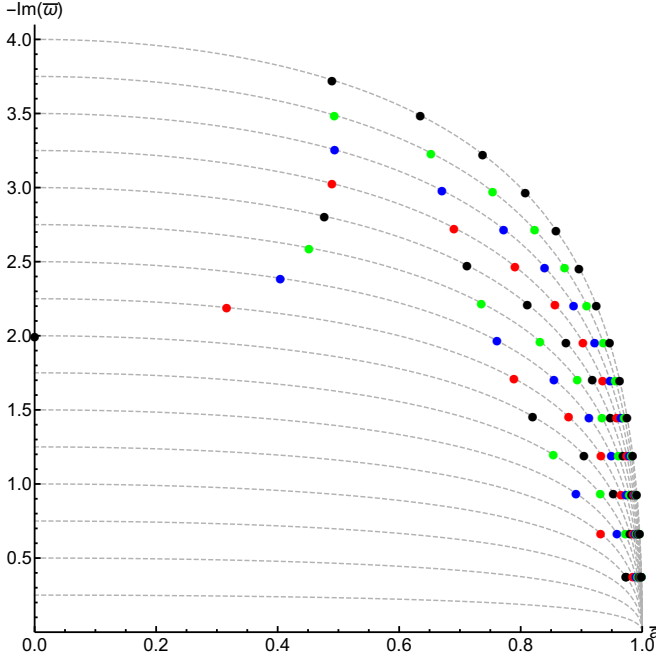


FIG. 19. Polynomial modes with $\bar{\omega} = \bar{\omega}_+$. The dashed gray lines are the possible values of $\bar{\omega}_+(N_+, \bar{a})$ for $1 \leq N_+ \leq 16$. The marker denote the discrete points where the $\Delta_{q+1} = 0$ condition is satisfied.

the phase information. When we look for polynomial solutions with $\bar{\omega} = \bar{\omega}_+$ and let $m \neq 0$, the determinant yields a complex number. When $m = 0$, or when we consider $\bar{\omega} = \bar{\omega}_-$, the determinant will be real. In either case, the phase information is important so that we have a smooth function across the zeros.

For the case of polynomial solutions with $\bar{\omega} = \bar{\omega}_+$, we choose the parameter set $\{\bar{\zeta}_+, \xi_-, \eta_+\}$ and use the coefficients from the recurrence relation associated with Eq. (9b) to build the matrix, explicitly replacing $\bar{\omega}$ with Eq. (27). We have carried out an extensive search for polynomial solutions (roots of the determinant or its proxy) for gravitational QNMs ($s = -2$).

First, we have found no evidence for polynomial solutions with $m \neq 0$. For all cases examined, the determinant moves around the complex plain as we vary \bar{a} , but never crosses the origin. However, for $m = 0$ we find what seems to be a countably infinite set of polynomial solutions. As expected, these solutions are not continuous, but occur at discrete values of \bar{a} . Figure 19 displays the solutions for $4 \leq N_+ \leq 16$. Notice that this figure differs from previous figures in that the horizontal axis measures \bar{a} instead of $\text{Re}(\bar{\omega})$ ($\text{Re}(\bar{\omega}) = 0$ for these solutions). In this figure, we have also plotted the constraint $\bar{\omega} = \bar{\omega}_+(N_+, \bar{a})$ as dashed gray lines for $1 \leq N_+ \leq 16$. The circular marks on each line denote the particular values of \bar{a} at which the $\Delta_{q+1} = 0$ condition is satisfied, marking a valid polynomial solution. We find no solutions for $N_+ < 4$. There is one solution for $N_+ = 4$, two for $N_+ = 5$, and so on to 4 solutions at $N_+ = 7$.

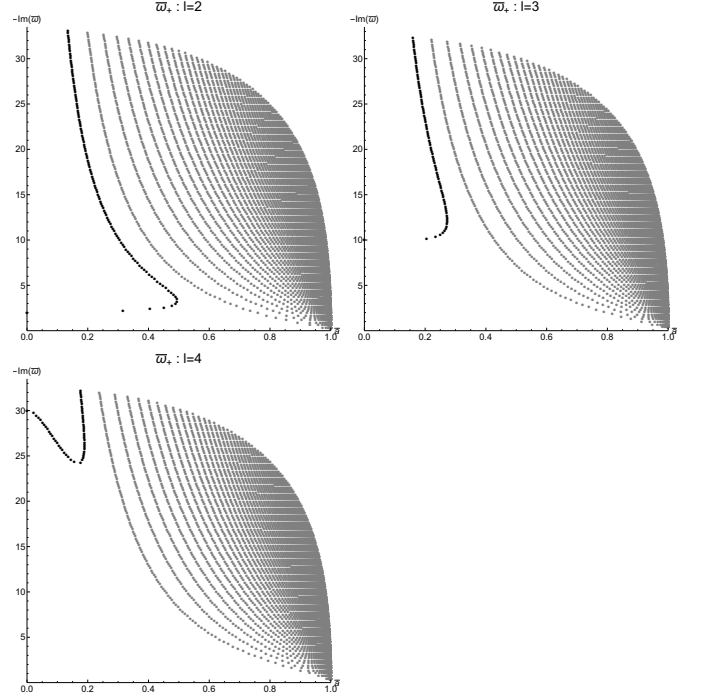


FIG. 20. Polynomial modes with $\bar{\omega} = \bar{\omega}_+$. The upper-left panel shows results for $\ell = 2$, the upper-right panel shows $\ell = 3$, and the lower-left $\ell = 4$. In each panel, the black dots are a subset of solutions that are shown in Sec. IV D to be polynomial solutions that are *simultaneously* QNMs and *TTM*_Ls. The gray dots are a subset of solutions that are shown to be *neither* QNM nor TTM.

At $N_+ = 8$, we find not 5, but 6 solutions. The jump in the number of solutions corresponds to the existence of a root for $\bar{a} = 0$. This is the mode corresponding to the algebraically special solution with $\bar{\omega} = \bar{\Omega}_2$. Between $8 \leq N_+ \leq 133$ we find $N_+ - 2$ solutions. We have not yet searched beyond $N_+ = 133$.

We have also carried out similar searches for $\ell = 3$ and $\ell = 4$. For $\ell = 3$ the first solution is found for $N_+ = 5$, while for $\ell = 4$, the first solution is found for $N_+ = 6$. Figure 20 shows individual plots for $\ell = 2, 3$, and 4. Each plot includes all of the solutions we have found up to $N_+ = 133$.⁶ We have omitted the lines denoting $\bar{\omega}_+$ for clarity.

For the case of polynomial solutions with $\bar{\omega} = \bar{\omega}_-$, we choose the parameter set $\{\bar{\zeta}_+, \xi_-, \eta_-\}$ and use the coefficients from the recurrence relation associated with Eq. (9b) to build the matrix, explicitly replacing $\bar{\omega}$ with Eq. (29). We have again carried out an extensive search for polynomial solutions for gravitational QNMs ($s = -2$).

As before, we have found no evidence of polynomial solutions with $m \neq 0$. For $m = 0$ we do find solutions,

⁶ We searched up to $N_+ = 132$ for $\ell = 3$, and $N_+ = 131$ for $\ell = 4$.

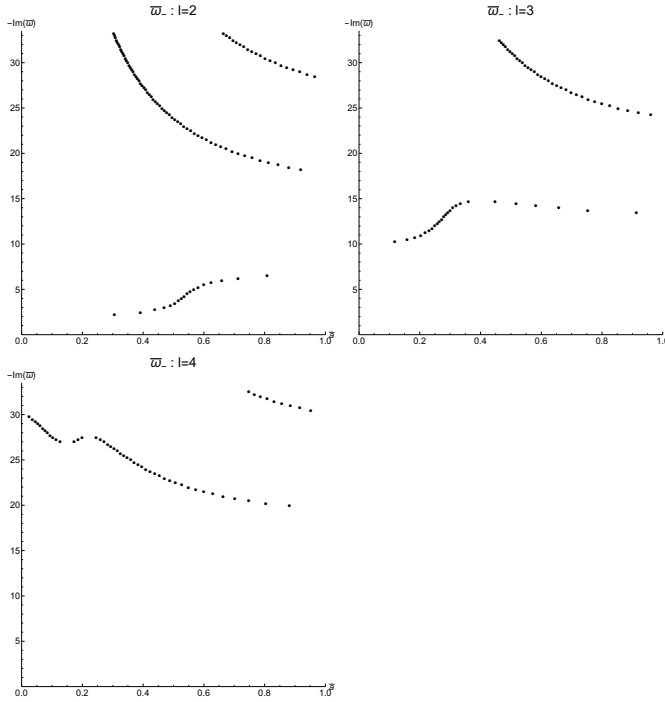


FIG. 21. Polynomial modes with $\bar{\omega} = \bar{\omega}_-$. The upper-left panel shows results for $\ell = 2$, the upper-right panel shows $\ell = 3$, and the lower-left $\ell = 4$. As shown in Sec. IV D, all of these polynomial solutions are QNMs.

but they appear to be less numerous. The solutions for $\ell = 2$ are seen in the upper-left plot of Fig. 21. We find no roots for $N_- < 9$, and for $9 \leq N_- \leq 26$ we find a single polynomial solution for each value of N_- . Between $27 \leq N_- \leq 72$ there appear to be no roots, but for $N_- \geq 73$ there seems to be at least one polynomial solution for each N_- . Starting at $N_- = 114$, we find a second polynomial solution for each N_- . While we have not extended our search beyond $N_- = 133$, it seems likely that the solutions persist indefinitely as N_- increases, and it would not be surprising to find even more solutions for each N_- as we move to larger N_- . Figure 21 also shows the result for $\ell = 3$ and 4. In these cases, the counting of the number of roots for each N_- is more complicated, but the behavior is clear from the figure.

Many, but not all of the polynomial solutions we have found correspond to specific modes on the QNM sequences that exist arbitrarily close to the NIA that we outlined in Sec. III B. Table II displays the QNM solutions we have found closest to the NIA for sequences that either appear to terminate on the NIA or emerge from the NIA. We noted that many of these seem to coincide with the $\bar{\omega} = \bar{\omega}_-$ constraint. Indeed, every $\ell = 2$, $m = 0$ sequence that is an overtone multiplet has one segment that corresponds precisely to one of the $\bar{\omega}_-$ polynomial solutions in the upper-left plot of Fig. 21 with $9 \leq N_- \leq 26$. The fact that we find no more polynomial solutions until $N_- = 73$ is why we are so confident that the $\ell = 2$, $m = 0$ QNM sequences we have computed with $n > 26$ are not

overtone multiplets. The beginning of this set of polynomial solutions also heralds the beginning of this set of overtone multiplets. However, the reason is a little more subtle, owing to the degeneracy between the $\bar{\omega}_+$ and $\bar{\omega}_-$ when $N_+ = N_- = 8$ and $\bar{a} = 0$.⁷

The remaining entries from Table II correspond precisely to certain polynomial solutions in the upper-left plot of Fig. 20. The left-most set of solutions, shown as black dots, starts with the algebraically special solution at $\bar{\omega} = -2i$ and $\bar{a} = 0$. The next 5 solutions move to the right and up slightly, then the remaining solutions move back leftward and up rapidly in the plot. After the algebraically special solution, the next 24 polynomial solutions correspond to the remaining entries from Table II. These $\bar{\omega}_+$ solutions, and the 18 $\bar{\omega}_-$ polynomial solutions discussed above, correspond to all of the $\ell = 2$, $m = 0$ QNM sequences we have computed which either terminate at or emerge from the NIA.

However, there are still several thousand instances where we have found looping solutions that encounter the NIA at a point of tangency. We have computed these for $\ell = 2, 3$, and 4 (see Figs. 16, 17, and 18; Tables III and IV). While we cannot compute a solution at the point of tangency using Leaver’s method, we can use quadratic interpolation to estimate the values of $\bar{\omega}$ and \bar{a} at the point of tangency. In every case, the interpolated result is in precise agreement with one of the $\bar{\omega}_+$ solutions shown as gray dots in Fig. 20.

All three plots in Fig. 20 contain a “left-most set” of solutions, shown as black dots, that starts at $\bar{a} = 0$ with $\bar{\omega} = \bar{\Omega}_\ell$. They also contain a large number of additional polynomial solutions that are grouped to the right of this set. Referring to Fig. 19, we see that this set of solutions breaks into roughly horizontal groups extending toward $\bar{a} = 1$, with a spacing in $\bar{\omega}$ of roughly $i/4$ between each grouping. The first group starts with $N_+ = 4$ and $\text{Im}(\bar{\omega}) \sim -i/2$, the second with $N_+ = 5$ and $\text{Im}(\bar{\omega}) \sim -3i/4$, and so on. Through $N_+ = 133$ we have found that once a horizontal grouping starts, it includes a member for every subsequent value of N_+ . In Fig. 19, the gray dashed lines represent $\bar{\omega}_+(N_+, \bar{a})$ for $1 \leq N_+ \leq 16$. It is clear that as we let N_+ increase, all of these curves will extend down to $\text{Im}(\bar{\omega}) = 0$ at $\bar{a} = 1$. It seems that each roughly horizontal grouping of solutions forms a countably infinite set, becoming arbitrarily dense as $\bar{a} \rightarrow 1$. Furthermore, the plots in Fig. 20 suggest that there is a countably infinite number of such roughly horizontal groupings of solutions, each itself countably infinite, for each value of ℓ .

We find that for each looping QNM sequence, each point of tangency corresponds precisely to a point in one of the roughly horizontal groupings. Figure 22 shows, for $\ell = 2$, the correspondence between all of the interpolated points of tangency and the polynomial solutions. For

⁷ In fact, as we will see in Sec IV D, this solution is “anomalous” at both $z = 0$ and $z = 1$

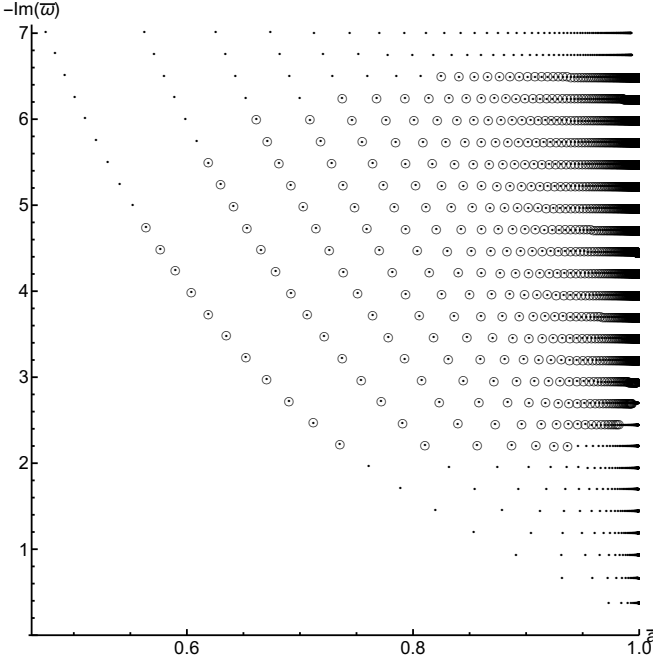


FIG. 22. Comparison of $\ell = 2$ polynomial modes with QNMs interpolated to the NIA. The open circles represent points where QNM sequences become tangent to the NIA. The points of tangency are determined by interpolation. The small solid dots are polynomial modes obeying $\bar{\omega} = \bar{\omega}_+$. Any mismatch in the centering of dots and circles is a graphing artifact. The maximum deviation has an absolute error of $\mathcal{O}(10^{-7})$. As shown in Sec. IV D, *none* of these polynomial solutions are QNMs or TTMs.

example, the seven points of tangency in the $\{2, 0, 9_1\}$ sequence (see Fig. 16 and Table III) correspond to the grouping that begins with $N_+ = 9$. The 20 points in the $\{2, 0, 10_1\}$ sequence correspond to the next grouping beginning with $N_+ = 10$. Since there are a finite number of points of tangency on each sequence, and an infinite number of polynomial solutions in each roughly horizontal grouping, only a small number of these polynomial solutions correspond to points along a QNM sequence. Similar behavior is seen for $\ell = 3$ and 4.

D. Generic, anomalous, and miraculous solutions

We have found two families ($\bar{\omega}_+$ and $\bar{\omega}_-$) of confluent Heun polynomial solutions on the NIA. The methods we have used have been tailored to finding QNMs. But we must be careful to examine, for each regular singular point, the behavior of the roots of the indicial equation to be certain that the solution actually represents a QNM.

Our methods for finding solutions, both Leaver's method and the method of confluent Heun polynomials, are based on power-series methods. When we consider the regular singular points at $z = 0$ and $z = 1$, standard Frobenius theory tells us that, when the roots of the in-

dicial equation differ by an integer, only the local series solution corresponding to the larger root is guaranteed to exist. The second local solution will usually include a log term. However, it is possible for the coefficient multiplying this log term to vanish. Subtleties can also occur at irregular-singular points, but that is not important in this work.

As seen in Eq. (9), the roots of the indicial equation for $z = 0$ are $\{0, 1 - \gamma\}$, and so we must be careful whenever γ is an integer. The behavior of solutions at the Cauchy horizon is associated with the η parameter, so it is not surprising that we can express γ as

$$\gamma = \gamma_{\pm} \equiv 1 + s + 2\eta_{\pm} = 1 \pm s \mp 2i\sigma_{-}. \quad (32)$$

In general, σ_{-} is complex and γ cannot be an integer. In fact, so long as $2i\sigma_{-}$ is not an integer (or a half-odd integer if s is a half odd integer), then γ cannot be an integer. This is the *generic* case. If $\bar{a} = 0$, then $\sigma_{-} = 0$ and γ is an integer (or zero) when s is an integer. This case has been examined by Maassen van den Brink[13]. Furthermore, if $m = 0$ and $\bar{\omega}$ is purely imaginary, then $2i\sigma_{-}$ will be an integer at that frequency for certain discrete values of \bar{a} . And if $m \neq 0$, special combinations of $\bar{\omega}$ and \bar{a} can allow $2i\sigma_{-}$ to be an integer. However, since the behavior of the solution at the Cauchy horizon is not relevant to determining if a mode is a QNM, we will not investigate this further.

The behavior of the solution at the event horizon, $z = 1$, is critical for determining if a mode is a QNM. As seen in Eq. (10), the roots of the indicial equation for $z = 1$ are $\{0, 1 - \delta\}$, and so we must be careful whenever δ is an integer. The behavior of solutions at the event horizon is associated with the ξ parameter, so it is not surprising that we can express δ as

$$\delta = \delta_{\pm} \equiv 1 + s + 2\xi_{\pm} = 1 \pm s \pm 2i\sigma_{+}. \quad (33)$$

In this case, solutions are *generic* so long as $2i\sigma_{+}$ is not an integer (or a half-odd integer if s is a half odd integer). From Eq. (19), we see that σ_{+} depends on $\bar{\omega}$ and \bar{a} . Rewriting this, we can find the frequencies that yield non-generic solutions:

$$\bar{\omega} = \frac{\bar{a}m - i(2i\sigma_{+})\sqrt{1 - \bar{a}^2}}{2(1 + \sqrt{1 - \bar{a}^2})}. \quad (34)$$

Comparing this to Eq. (27), we see that the equations are identical with $2i\sigma_{+} = N_+$. So, *any confluent Heun polynomial solution obeying the constraint that $\bar{\omega} = \bar{\omega}_+$ is non-generic at the event horizon* for any choice of s . Thus, for the majority of the gravitational, $s = -2$, polynomial modes on the NIA which we have found, we cannot immediately conclude that they are QNMs.

Before we explore this further, we should consider the case of polynomial solutions obeying the constraint that $\bar{\omega} = \bar{\omega}_-$. In this case, if $\bar{a} = 0$ and if s is an integer, then the mode is non-generic. Again, this case has been examined by Maassen van den Brink[13]. If $\bar{a} \neq 0$ but

$m = 0$, then a mode can be non-generic if $\frac{N_+(1+\sqrt{1-\bar{a}^2})}{2\sqrt{1-\bar{a}^2}}$ is an integer when s is an integer (or a half-odd integer when s is a half-odd integer). All of the confluent Heun polynomial solutions on the NIA that we have computed so far that obey the $\bar{\omega} = \bar{\omega}_-$ constraint *do not satisfy this condition*. While each such mode must be tested individually, so far, all have proven to be generic and we can conclude that *all of the $\bar{\omega} = \bar{\omega}_-$ polynomial solutions* (see Fig. 21) *are QNMs*.

1. Non-generic modes

Let us now consider the behavior at the event horizon ($z = 1$) of non-generic modes on the NIA. All of these modes have $\bar{\omega} = \bar{\omega}_+$ and are characterized by the parameter $N_+ = 2i\sigma_+$ (see Fig. 20). The two possible local behaviors of these non-generic modes on the NIA are either $(z-1)^{-s-N_+/2}$, which we would naively associate with modes propagating into the horizon, and $(z-1)^{N_+/2}$, which we would expect to be modes propagating out from the horizon. Frobenius theory tells us that two possibilities exist for non-generic solutions. The simplest case is that the only series solution (and it is a truncated series for our polynomial solutions) has leading behavior associated with the largest exponent. For $N_+ > -s$, this is $(z-1)^{N_+/2}$. The other series solution (and it need not be truncated) will have leading behavior $(z-1)^{-s-N_+/2}$, but will also include a term that is proportional to $\ln(z-1)$ multiplied by the first solution. Maassen van den Brink labels this non-generic case as “anomalous” [13] and argues that the second solution including the $\ln(z-1)$ term cannot represent a mode propagating into the horizon. Surprisingly, he finds that the series solution, which appears to correspond to a TTM_L , simultaneously represents a QNM and a TTM_L . In Fig. 20, all “anomalous” solutions are displayed with a black dot. We will return to discuss this in more detail below.

The second possible non-generic behavior occurs when the coefficient multiplying the $\ln(z-1)$ happens to vanish. Maassen van den Brink labels this *doubly* non-generic case as “miraculous”. In this case, our polynomial solutions can have leading behavior $(z-1)^{-s-N_+/2}$. However, unlike the generic case, this does not guarantee that our solution is a QNM. Because a term like $(z-1)^{N_+/2}$ can be part of the same solution, the polynomial solution may be a linear combination of ingoing and outgoing modes at the horizon. If so, then our solution is neither a QNM nor a TTM_L . In Fig. 20, all “miraculous” solutions are displayed with a gray dot. These behaviors are, to say the least, counter-intuitive. To understand the implications of these two possibilities, it is useful to view them from the perspective of scattering theory.

Begin with a free mode propagating into the horizon at $z = 1$ and then construct an n^{th} -order Born approximation keeping $\bar{\omega}$ and \bar{a} unspecified. Let us denote the Born series solution for this *outgoing* mode as $R_-(z, \bar{\omega}, \bar{a})$. Since we are only concerned with the behavior near the

horizon, we need only construct the Born approximation locally. This can be simply constructed using the recurrence relation, Eq. (8a), for the local solution (10b) with the parameter choice $\{\bar{\zeta}_+, \xi_+, \eta_+\}$. For example, the 3rd-order local Born approximation would be

$$R_-^{(3)}(z, \bar{\omega}, \bar{a}) \sim (z-1)^{-s-i\sigma_+} \left[1 - \frac{g_0}{f_0}(1-z) + \frac{g_0g_1 - f_0h_1}{f_0f_1}(1-z)^2 - \frac{g_0g_1g_2 - f_0h_1g_2 - g_0f_1h_2}{f_0f_1f_2}(1-z)^3 \right] \quad (35)$$

The denominator of the n^{th} -order Born approximation is $\prod_{i=0}^{n-1} f_i$, and we must consider when this can vanish. From Eq. (8c), we see that $f_k^{(a)}$ will vanish if $k = -\gamma$. In Eq. (6), γ is the third parameter, but in Eq. (10b) the third parameter is δ . For our parameter choice, $\delta = 1 - s - 2i\sigma_+$, with σ_+ is a function of $\bar{\omega}$ and \bar{a} . Recall that any time $\bar{\omega} = \bar{\omega}_+$, we find that $2i\sigma_+ = N_+$ and δ is an integer. In summary, whenever $\bar{\omega} = \bar{\omega}_+$ with $N_+ > -s$, δ is a non-positive integer and $f_{-\delta}^{(a)} = 0$ causing the $(1-\delta)^{\text{th}}$ -order and higher terms in the Born approximation to have a vanishing denominator.

As we saw above, Frobenius theory tells us that our solution is non-generic at $z = 1$ if δ is an integer. Moreover, $(z-1)^\delta$ corresponds to the smaller root of the indicial equation when δ is a negative integer. So, our non-generic solutions correspond to the case where the denominator vanishes in the $(1-\delta)^{\text{th}}$ -order and higher terms in the Born series.

Of course, there are two types of non-generic behavior. We first consider the “anomalous” case. As Maassen van den Brink has shown [13], the vanishing denominator means the mode propagating into the black hole scatters so strongly off of the potential tail as it approaches the event horizon that the normally dominant behavior of the outgoing mode is overwhelmed and the outgoing mode has exactly the same local behavior as the incoming mode. More precisely, in the *anomalous case*, the mode propagating into the black holes behaves like

$$R_-^{(A)}(z, \bar{a}) \sim \lim_{\bar{\omega} \rightarrow \bar{\omega}_+} f_{-\delta}^{(a)} R_-(z, \bar{\omega}, \bar{a}), \quad (36)$$

The Born series for the mode traveling out of the black hole can be constructed in a similar way using the parameter choice $\{\bar{\zeta}_+, \xi_+, \eta_+\}$. Let us denote the Born series solution for this *incoming* mode as $R_+(z, \bar{\omega}, \bar{a})$. For the anomalous solutions, we find that $R_-^{(A)}(z, \bar{a}) \propto R_+(z, \bar{\omega}_+, \bar{a})$. Hence, the *anomalous solutions are simultaneously QNMs and TTM_L s*.

For the “miraculous” case, in addition to the denominator of the n^{th} -order Born approximation vanishing, we find that the numerator also vanishes. The value of the coefficient of the n^{th} -order term in the Born series is obtained by taking the limit as $\bar{\omega} \rightarrow \bar{\omega}_+$ and $\bar{a} \rightarrow \bar{a}_p$, where \bar{a}_p is the angular momentum parameter of the polynomial mode. The result for the n^{th} coefficient depends

on the order in which the limits are taken, however the conclusion is the same regardless of the ordering. By definition[13], in the *miraculous case*, the mode propagating into the black hole behaves like

$$\mathbf{R}_-^{(M)}(z) \sim \lim_{\bar{\omega} \rightarrow \bar{\omega}_+} \left(\lim_{\bar{a} \rightarrow \bar{a}_p} R_-(z, \bar{\omega}, \bar{a}) \right). \quad (37)$$

Interestingly, we find that the Born series $\mathbf{R}_-^{(M)}(z)$ *does not terminate* when $\bar{\omega}_+$ and \bar{a} correspond to our confluent Heun polynomial solutions. Instead, it is a linear combination, $\mathbf{R}_-^{(M)}(z) + C_M R_+(z, \bar{\omega}_+, \bar{a}_p)$, that terminates. In fact, the same is true if the limits are taken in the reverse order, except that C_M changes. So the commutation of the limits gives

$$\lim_{\bar{\omega} \rightarrow \bar{\omega}_+} \lim_{\bar{a} \rightarrow \bar{a}_p} R_-(z, \bar{\omega}, \bar{a}) - \lim_{\bar{a} \rightarrow \bar{a}_p} \lim_{\bar{\omega} \rightarrow \bar{\omega}_+} R_-(z, \bar{\omega}, \bar{a}) \quad (38)$$

$$\propto R_+(z, \bar{\omega}_+, \bar{a}_p).$$

We should point out that the non-terminating Born series $\mathbf{R}_-^{(M)}(z)$ and $R_+(z, \bar{\omega}_+, \bar{a}_p)$ are both local series solutions. We have seen for QNM solutions on the NIA, a confluent Heun function cannot exist (ie the series will not converge) unless the series terminates. A similar argument holds for TTM_L solutions⁸, and so neither of the Born series are convergent for large z .

As a concrete example of this, consider the case with $N_+ = 5$. A polynomial solution is found when $\bar{a} = 0.931905$ with $_{-2}A_{20} = 4.199325$. The radial solution is

$$R_{51}(z) = z^{\eta_+} (z-1)^{-1/2} e^{(\bar{r}_+ - \bar{r}_-) \bar{\zeta}_+ z} \left(1 + 1.06819(1-z) + 0.580484(1-z)^2 + 0.191606(1-z)^3 + 0.117043(1-z)^4 + 0.0337923(1-z)^5 + 0.0200664(1-z)^6 \right). \quad (39)$$

The first few terms of the local Born series for the outgoing mode are

$$\mathbf{R}_-^{(M)}(z) = (z-1)^{-1/2} \left(1 + 1.06819(1-z) + 0.580484(1-z)^2 - 20.425330(1-z)^3 + 47.821179(1-z)^4 - 42.3949518(1-z)^5 + 14.5536633(1-z)^6 - 0.6166794(1-z)^7 + \dots \right), \quad (40)$$

while the first few terms of the local Born series for the incoming mode are

$$R_+(z) = (z-1)^{5/2} \left(1 - 2.313832(1-z) + 2.0546777(1-z)^2 - 0.7049349(1-z)^3 + 0.0299113(1-z)^4 + \dots \right). \quad (41)$$

We find that $R_{51}(z) \sim \mathbf{R}_-^{(M)}(z) + 20.616936 R_+(z)$ with all terms of order $(z-1)^{13/2}$ and higher canceling.

At $z = 1$, $R_{51}(z)$ behaves as a linear combination of an incoming and an outgoing mode, and by itself cannot be a QNM. However, if a TTM_L mode exists at the same values of $\bar{\omega}$ and \bar{a} , we could take a linear combination of $R_{51}(z)$ with this mode to remove the incoming mode behavior at $z = 1$ without introducing an incoming mode at infinity. Given the explicit, closed form solution $R_{51}(z)$ for the radial function, we can construct a second, linearly independent solution $\tilde{R}(z) = v(z) R_{51}(z)$ to the radial Teukolsky equation. Using standard methods, we can obtain $v(z)$ as an integral and determine the local behavior of $\tilde{R}(z)$ at both $z = 1$ and $z = \infty$. We find that $\lim_{z \rightarrow 1} \tilde{R}(z) \sim R_+(z)$, representing an incoming mode at the event horizon. At infinity, $\tilde{R}(z)$ also corresponds, to an *incoming* mode, although the solution seems ill-behaved here. Thus, $\tilde{R}(z)$ is *not* a TTM_L mode and we must conclude that no QNM or TTM_L modes exists at the values of $\bar{\omega}$ and \bar{a} associated with $R_{51}(z)$.

We have performed the same analysis for numerous cases of “miraculous” polynomial solutions (gray dots in Fig. 20) and have found the same result in each case. This does not prove that the “miraculous” cases are not QNMs (or TTM_Ls) in all cases. It is possible that under certain circumstances $\mathbf{R}_-^{(M)}(z)$ itself terminates and contains no contribution from $R_+(z)$. However, we conjecture that whenever $\mathbf{R}_-^{(M)}(z)$ does not terminate, the “miraculous” solutions are neither QNMs nor TTM_Ls.

While examining the Born series is helpful in understanding the behavior of the anomalous and miraculous solutions, it is somewhat simpler to determine their behavior by examining the properties of the coefficient matrix, (13), used to locate the Heun polynomial solutions. For clarity, we will illustrate this for the specific cases discussed above. Assume that we choose the parameter set $\{\bar{\zeta}_+, \xi_-, \eta_+\}$ and use the local solution of Eq. (10b) to construct the coefficient matrix. For the case of $\bar{\omega} = \bar{\omega}_+$, the upper-left block of (13) will be a $(q+1) \times (q+1)$ -dimensional tridiagonal matrix. As outlined above, we can easily see that the coefficient $f_{-\delta}^{(a)} = 0$, and so long as $s < 0$ this vanishing element will be part of the upper-left block of (13). This submatrix takes the block form

$$\begin{bmatrix} g_0 & f_0 & 0 & \cdots & 0 & 0 & 0 & \cdots & 0 \\ h_1 & g_1 & f_1 & \ddots & 0 & 0 & 0 & \cdots & 0 \\ 0 & \ddots & \ddots & \ddots & \ddots & \ddots & \ddots & \ddots & \vdots \\ 0 & \ddots & h_{-\delta} & g_{-\delta} & 0 & 0 & 0 & \cdots & 0 \\ \hline 0 & \cdots & 0 & h_{1-\delta} & g_{1-\delta} & f_{1-\delta} & 0 & \cdots & 0 \\ 0 & \cdots & 0 & 0 & h_{2-\delta} & g_{2-\delta} & f_{2-\delta} & \ddots & \vdots \\ \vdots & \ddots & \vdots & \vdots & \ddots & \ddots & \ddots & \ddots & 0 \\ 0 & \cdots & 0 & 0 & 0 & 0 & h_{q-1} & g_{q-1} & f_{q-1} \\ 0 & \cdots & 0 & 0 & 0 & 0 & 0 & h_q & g_q \end{bmatrix}, \quad (42)$$

⁸ To consider TTM_Ls, we follow the method of Sec. IV B, but let $\xi = \xi_+$. p remains unchanged and only u_2 in Eq. (23) is different. This term has no effect on the convergence argument.

with $q = N_+ - s - 1$ and $-\delta = q + 2s$. Because of its tridiagonal form and the vanishing of the off-diagonal element $f_{-\delta}^{(a)}$, it is easy to see that the determinant of the matrix (42) can be written as the product of the determinants of the two diagonal block elements[28]. To simplify the discussion, let us denote the determinant of the upper-left diagonal block as Δ_u and the determinant of the lower-right diagonal block as Δ_d . So, the necessary and sufficient condition for a polynomial solution can be written as $\Delta_{q+1} = \Delta_u \Delta_d = 0$.

First, consider the case when $\Delta_d = 0$ while $\Delta_u \neq 0$. Because $\Delta_u \neq 0$, the first $1 - \delta = N_+ + s$ coefficients, $c_k^{(a)}$, of Eq. (6) must vanish. The next $-2s$ coefficients, $c_k^{(a)}$ with $1 - \delta \leq k \leq q$, associated with the lower-right block need not vanish. The vector of values for $c_k^{(a)}$ can be determined using standard matrix methods. We are free to normalize this solution vector so that $c_{1-\delta}^{(a)} = 1$. If we were to simply evaluate the coefficients directly via the recurrence relation, we would find that

$$c_{1-\delta}^{(a)} = \frac{\Delta_u}{\prod_{i=0}^{-\delta} f_i}. \quad (43)$$

Since $\Delta_u \neq 0$ and $f_{-\delta}^{(a)} = 0$, $c_{1-\delta}^{(a)}$ diverges. This is the “anomalous” case, but computing the coefficients via matrix methods automatically rescales the solution as in Eq. (36).

We have seen that an anomalous solution is simultaneously a QNM and a TTM_L , so it is not surprising that the lower-right block of (42) is a $(-2s) \times (-2s)$ matrix with coefficients that are identical to the coefficients of one of the matrices that can be constructed to consider TTM_L polynomial solutions. To construct this matrix, we continue to use Eq. (10b), but change the choice of ξ to ξ_+ . The local solution is now associated with modes propagating out from the event horizon. The necessary condition for a polynomial solution in this case is $q = -1 - 2s$ (see Ref.[16] for details). While this condition does not constrain $\bar{\omega}$, we may choose to look for solutions when $\bar{\omega} = \bar{\omega}_+$. Under these conditions, the matrix is identical to the lower-right block of (42).

Now consider the reverse situation in which $\Delta_d \neq 0$ while $\Delta_u = 0$. In this case, we can determine the first $1 - \delta = N_+ + s$ coefficients, $c_k^{(a)}$, of Eq. (6) using standard matrix methods. The matrix element $h_{1-\delta}^{(a)}$ in the lower-left block cannot vanish because we have chosen N_+ so that $h_{q+1}^{(a)} = 0$, and from Eq. (8d) it is clear that only one coefficient $h_k^{(a)}$ can vanish unless they all vanish with $p = 0$. Now, so long as $\Delta_d \neq 0$, there exists a unique solution for the remaining $-2s$ coefficients, $c_k^{(a)}$. If we again simply evaluate the coefficients directly via the recurrence relation, $\Delta_u = f_{-\delta}^{(a)} = 0$ means that we must evaluate Eq. (43) in the limit as in Eq. (37). This is the “miraculous” case. However, the value of $c_{1-\delta}^{(a)}$ computed via matrix methods will not, in general, equal the limit value of Eq. (43). When the values differ, the behavior

local to $z = 1$ is a linear combination of incoming and outgoing modes.

What if the determinants of both diagonal blocks vanish? First, it is not clear that the “miraculous” solution will persist in this case. If it could, then the vanishing of the determinant of the lower-right block implies that a polynomial TTM_L mode also exists. As discussed earlier, the existence of a TTM_L solution in addition to a “miraculous” solution would guarantee that we could construct a QNM through a linear combination of these solutions. This would give us two linearly independent polynomial solutions, one a QNM and one a TTM_L . If the “miraculous” solution does not persist, then the solution reverts to being of “anomalous” type.

V. SUMMARY AND DISCUSSION

The main goal of this paper has been to understand when QNMs can exist with frequencies precisely on the NIA. We have shown that there exist countably infinite sets of QNMs with frequencies on the NIA. These exist in two distinct families. The first family obeys the constraint in Eq. (29) that $\bar{\omega} = \bar{\omega}_-$. It seems that all of these polynomial solutions are “generic”⁹ and correspond to QNMs with purely imaginary frequencies. Examples of this family of modes, for $\ell = 2, 3$, and 4 , are displayed in Fig. 21. The second family obeys the constraint in Eq. (27) that $\bar{\omega} = \bar{\omega}_+$. All of these modes are “non-generic” and split into two types. One type is “anomalous”, in which case each polynomial solution corresponds simultaneously to a QNM and a TTM_L . The second type is “miraculous”, in which case each polynomial solution is neither a QNM nor a TTM. Examples of both types of this family of modes, for $\ell = 2, 3$, and 4 , are displayed in Fig. 20. There are additional interesting points to consider for each case.

A. The anomalous cases

It has been known for some time that the algebraically special modes of Schwarzschild (see Eq. (4)) are simultaneously QNMs and TTM_L s. This was proven by Maassen van den Brink[13] by exploiting the supersymmetric relationship between the Regge-Wheeler[9] and Zerilli[14] equations for the odd- and even-parity gravitational perturbations of Schwarzschild. More precisely, he found that the frequencies $\bar{\Omega}_\ell$ yielded solutions that were simultaneously QNMs and TTM_L s when considering the Zerilli equation, but that the Regge-Wheeler equation had no QNM or TTM solutions at this frequency. The

⁹ Our methods do not rule out the possibility that a particular solution could be non-generic. However, we have not encountered any.

latter proving that there are no TTM_R modes for the algebraically special frequencies of Schwarzschild. In terms of the Teukolsky equation, he was able to show the analogous result in the limit that $\bar{a} = 0$. Specifically, for $s = -2$ the algebraically special modes of Schwarzschild are simultaneously QNMs and TTM_L s, while for $s = +2$ they do *not* correspond to TTM_R s. However, in considering the extension of these arguments to $0 < \bar{a} < 1$, his approach lead him to conclude that the algebraically special modes were all of generic type for $\bar{a} > 0$.

Using the theory of confluent Heun polynomials, we have shown conclusively that this is not true. The *anomalous* cases of $\bar{\omega} = \bar{\omega}_+$ (black dots in Fig. 20) are all discrete algebraically special modes with $\bar{a} > 0$. As we discussed in Sec. IV D 1, for the anomalous case, the determinant Δ_d vanishes and this is identical to the $\Delta_{q+1} = 0$ condition when considering TTM_L s. We have shown in Ref.[16], that this is identical to the vanishing of the square of the Starobinski constant which is the equation satisfied by the algebraically special modes for all values of \bar{a} [10].

We find, then, that the $m = 0$ algebraically special modes have a particularly interesting behavior. Chandrasekhar[10] provided the first table of the mode frequencies for $\bar{a} > 0$, showing that the $\ell = 2, m = 0$ mode frequencies moved along the NIA (at least initially) as \bar{a} increased. Onozawa[12] plotted in his Fig. 7 the $\ell = 2, m \geq 0$ algebraically special mode frequencies. In this plot it is clear that when $\bar{a} \sim 0.494446$, the $m = 0$ sequence turns off of the NIA and the mode frequencies are complex. This plot was extended to show similar behavior for the $\ell = 3$ modes as well in Fig. 24 of Ref.[16]. Comparing this to the behavior of the anomalous points (black dots) in Fig. 20, we see that the first few points, starting at $\bar{\Omega}_\ell$ and moving to the right (increasing \bar{a}) correspond to specific points along the algebraically special sequences as they move along the NIA. While each mode frequency along the sequence represents, in general, a TTM_L , at these particular points, the mode is simultaneously a QNM and a TTM_L .¹⁰

The anomalous polynomial mode frequencies with the largest values of \bar{a} correlate with the point where the algebraically special sequences turn off of the NIA as \bar{a} increases. But, Fig. 20 shows something else that is new. *There is a second branch of the algebraically special modes which, to our knowledge, has never before been noticed.* To be clear, let us consider the case of the $\ell = 2, m = 0$ algebraically special modes. The sequence begins at $\bar{\omega} = \bar{\Omega}_2$ with $\bar{a} = 0$. For $0 < \bar{a} \lesssim 0.494446$, $-\text{Im}(\bar{\omega})$ increases toward $\bar{\omega} \sim -3.3308i$. At this point, if \bar{a} increases, the sequence moves off of the NIA. But, *there is a new branch of the sequence moving along the NIA with*

$-\text{Im}(\bar{\omega})$ increasing beyond this point as \bar{a} decreases back to zero. Numerical evidence shows that this new branch of the algebraically special modes behaves as an inverse-power law in \bar{a} . So, we find that for $0 < \bar{a} \lesssim 0.494446$, there are two distinct sequences of algebraically special modes which together have frequencies that cover the entire NIA below $-2i$. And, at a countably infinite number of frequencies, the $s = -2$ modes become anomalous. These anomalous solutions correspond with points where the $m = 0$ QNM frequency sequences terminate at (or emerge from) the NIA. At all of these points, the $s = -2$ mode is simultaneously a QNM and a TTM_L , but the $s = +2$ mode is not a TTM_R .

Similar behavior is seen for the $\ell = 3, m = 0$ algebraically special modes. However, Fig. 20 shows that the $\ell = 4$ case is a bit more complicated. It suggests that the algebraically special mode frequencies will first move to smaller values of $-\text{Im}(\bar{\omega})$, then reverse course and increase, as \bar{a} is increased. Following the point where continuing to increase \bar{a} causes the mode frequencies to move off of the NIA, we see the same behavior of the mode frequencies where they continue to moving along the NIA as \bar{a} decreases again toward zero.

B. The miraculous cases

The miraculous subset of the $\bar{\omega} = \bar{\omega}_+$ polynomial solutions seem to represent a new and unusual set of modes. They are neither QNM nor TTM unless some third level of non-generic behavior intervenes to make them anomalous, and this has not been seen so far. These solutions are countably infinite, with a possibly finite number of them (see Fig. 22) for each ℓ corresponding to points along certain QNM sequences that become tangent to the NIA. For every $m = 0$ looping QNM sequence we have seen (see Figs. 16, 17, and 18), *each point of tangency with the NIA represents a point that must be missing from that QNM sequence.*

Two recent papers[17, 19] have claimed to find gravitational QNMs with frequencies on the NIA. We have shown that no actual QNMs exist with frequencies on the NIA at frequencies corresponding to their solutions. However, in both cases there is some correlation with our “miraculous” solutions. In the first paper[17], using both WKB and matched-asymptotic-expansion methods, the authors find an approximation for $\bar{\omega}$ for what they refer to as zero damped modes (ZDMs) and damped modes (DMs). With $\epsilon \equiv 1 - \bar{a}$, and with $m = 0$, they find $\bar{\omega} \approx -i(n + 1/2)\sqrt{\epsilon/2}$. If we consider $\bar{\omega}_+$ in the limit that $\bar{a} \rightarrow 1$, then we find $\bar{\omega}_+ \approx -iN_+\sqrt{\epsilon/2}$. As Fig. 19 makes clear, for $N_+ \gg 1$ there are a large number of curves with small $-\text{Im}(\bar{\omega})$ as we approach $\bar{a} \sim 1$. Clearly, the difference between $n + 1/2$ and N_+ is small for large $n = N_+$, so their approximation can be a reasonably good approximation for our necessary (but not sufficient) condition for having a polynomial QNM solution with a purely imaginary frequency. In the second paper[19], the

¹⁰ Along the corresponding $s = +2$ sequence of algebraically special modes, in general each mode is TTM_R . However, as with the $\bar{a} = 0$ case, modes at the same set of frequencies are “miraculous” and are *not* TTM_R s.

author uses a more tailored matched asymptotic expansion to find $m = 0$ resonances in the limits that $\bar{a} \approx 1$ and $-\text{Im}(\bar{\omega})$ is small. His result is nearly identical with our expression for $\bar{\omega}_+$, except that N_+ is replaced by $\ell + 1 + n$. Here, n is an integer and if ℓ were simply our harmonic index, the result would be essentially identical to ours. However, in this case ℓ is the integer harmonic index *plus* a non-integer correction. Never-the-less, the correction is small, and we again find that his resonance is a good approximation for our necessary (but not sufficient) condition for having a polynomial QNM solution with a purely imaginary frequency.

Clearly, only the “miraculous” modes are reasonably close to either of the claimed solutions with frequencies on the NIA. But we have seen that none of these modes are QNMs. The authors of Ref. [17] offered additional evidence that they had found QNMs with a purely imaginary frequency by finding numerical solutions which seemed consistent with their approximate expressions for those frequencies. However, in finding numerical solutions with frequencies on the NIA, the authors used Leaver’s continued fraction method on the NIA. As we have shown in Sec. IV B, the continued fraction does not converge when evaluated with a frequency on the NIA and cannot be used to locate QNMs.

In Ref. [19], the author’s finding of a continuum of QNMs for $\bar{a} \sim 1$ is accompanied by a continuum of “total reflection modes” that correspond to our TTM_L s. These nearly coinciding QNM/ TTM_L pairs seem like good approximations for the anomalous QNM/ TTM_L solutions we have found, except that we find no such solutions in the small $\bar{\omega}$, large \bar{a} limit in which the author’s approximations are valid. It could be very informative to understand why these analytic approximation methods both seem to find QNM solutions when none exist. At present, we do not have a clear understanding of this. It seems clear that both methods are finding a reasonable approximation of the necessary condition that $\bar{\omega} = \bar{\omega}_+$. However, neither seems to incorporate anything analogous to the $\Delta_{q+1} = 0$ condition to restrict the solutions. Perhaps more to the point, none of these approximate methods deal with the very subtle aspects of determining the nature of the solution at the horizon boundary when the solutions are non-generic.

ACKNOWLEDGMENTS

We would like to thank Emanuele Berti, Aaron Zimmerman, and Shahar Hod for helpful discussions.

-
- [1] R. P. Kerr, Phys. Rev. Lett. **11**, 237 (1963).
 - [2] S. A. Teukolsky, Classical Quantum Gravity **32**, 124006 (2015).
 - [3] E. Berti, V. Cardoso, and A. O. Starinets, Classical Quantum Gravity **26**, 163001 (2009).
 - [4] H.-P. Nollert, Classical Quantum Gravity **16**, R159 (1999).
 - [5] B. P. Abbott *et al.* (LIGO Scientific Collaboration and Virgo Collaboration), Phys. Rev. Lett. **116**, 061102 (2016).
 - [6] B. P. Abbott *et al.* (LIGO Scientific Collaboration and Virgo Collaboration), Phys. Rev. Lett. **116**, 241103 (2016).
 - [7] S. Hod, Phys. Rev. Lett. **81**, 4293 (1998).
 - [8] E. W. Leaver, Proc. R. Soc. A **402**, 285 (1985).
 - [9] T. Regge and J. A. Wheeler, Phys. Rev. **108**, 1063 (1957).
 - [10] S. Chandrasekhar, Proc. R. Soc. A **392**, 1 (1984).
 - [11] N. Andersson, Classical Quantum Gravity **11**, L39 (1994).
 - [12] H. Onozawa, Phys. Rev. D **55**, 3593 (1997).
 - [13] A. Maassen van den Brink, Phys. Rev. D **62**, 064009 (2000).
 - [14] F. J. Zerilli, Phys. Rev. Lett. **24**, 737 (1970).
 - [15] E. Berti, V. Cardoso, K. D. Kokkotas, and H. Onozawa, Phys. Rev. D **68**, 124018 (2003).
 - [16] G. B. Cook and M. Zalutskiy, Phys. Rev. D **90**, 124021 (2014).
 - [17] H. Yang, F. Zhang, A. Zimmerman, D. A. Nichols, E. Berti, and Y. Chen, Phys. Rev. D **87**, 041502(R) (2013).
 - [18] H. Yang, A. Zimmerman, A. Zenginoğlu, F. Zhang, E. Berti, and Y. Chen, Phys. Rev. D **88**, 044047 (2013).
 - [19] S. Hod, Phys. Rev. D **88**, 084018 (2013).
 - [20] G. B. Cook and M. Zalutskiy, (2016), submitted, arXiv:1603.09710 [gr-qc].
 - [21] S. A. Teukolsky, Astrophys. J. **185**, 635 (1973).
 - [22] P. Fiziev and D. Staicova, Phys. Rev. D **84**, 127502 (2011).
 - [23] P. T. Leung, A. Maassen van den Brink, K. W. Mak, and K. Young, Classical Quantum Gravity **20**, L217 (2003).
 - [24] A. Ronveaux, ed., *Heun’s Differential Equations* (Oxford University, New York, 1995).
 - [25] R. S. Borissov and P. P. Fiziev, Bulg. J. Phys. **37**, 65 (2010).
 - [26] E. W. Leaver, J. Math. Phys. (N.Y.) **27**, 1238 (1986).
 - [27] W. Gautschi, SIAM Rev. **9**, 24 (1967).
 - [28] M. E. El-Mikkawy, Appl. Math. Comp. **150**, 669 (2004).